

Spin-Orbit Semimetals in the Layer Groups

Benjamin J. Wieder and C. L. Kane

Department of Physics and Astronomy, University of Pennsylvania, Philadelphia, PA 19104

Recent interest in point and line node semimetals has lead to the proposal and discovery of these phenomena in numerous systems. Frequently, though, these nodal systems are described in terms of individual properties reliant on specific space group intricacies or band-tuning conditions. Restricting ourselves to cases with strong spin-orbit interaction, we develop a general framework which captures existing systems and predicts new examples of nodal materials. In many previously proposed systems, the three-dimensional nature of the space group has obscured key generalities. Therefore, we show how within our framework one can predict and characterize a diverse set of nodal phenomena even in two-dimensional systems constructed of three-dimensional sites, known as the “Layer Groups”. Expanding on an existing discussion by Watanabe, Po, Vishwanath, and Zaletel of the relationship between minimal insulating filling, nonsymmorphic symmetries, and compact flat manifolds, we characterize the allowed semimetallic structures in the layer groups and draw connections to related three-dimensional systems.

PACS numbers: 74.45.+c, 71.10.Pm, 74.78.Fk, 74.78.Na

I. INTRODUCTION

Nodal semimetals are characterized by single points where the valence and conduction bands meet. The existence of these points at the Fermi energy has implications for bulk transport, surface physics, and is even related to topology^{1–7}. Since the discovery of nodal points with linear dispersion in single-sheet graphene^{8,9}, there has been great effort to locate and characterize similar band-touching nodes in other systems. Rich nodal physics can also be found in graphene bilayers, however these systems have quadratically-dispersing nodes, and thus differing transport properties and gapped phases^{10–16}. Therefore, this search for graphene-like physics can be considered more specifically a search for systems with *linearly-dispersing* nodal points at the Fermi energy.

Extending to three dimensions, there are generically two realizations of this nodal physics: point nodes and nodal lines. Bands can meet at nodes with linear dispersion in three directions and form Dirac or Weyl points, with four- and two-fold nodal degeneracies respectively^{17–30}, or in unusual three-, six-, and eight-fold degeneracies^{31,32}. Bands can also meet and form line nodes, or lines along which there is no dispersion in one direction and linear dispersion in the remaining two directions^{33–44}.

Each of these examples of nodal phenomena owes its protection to some combination of topology and exact crystalline symmetries. However, many of them have been described in terms of individual properties, such as topological invariants and symmetry eigenvalues. In this manuscript, we seek to provide a more generalized consideration of those nodal systems protected by crystalline symmetries, as well as a means to sort and classify them.

A. The Two Flavors of Semimetals

As a starting point for sorting these various nodal materials, one could ask whether or not any of their nodal features can be eliminated to open a gap. Consider the ability to remove point nodes pairwise, or to close and gap line nodes at a point, but without reducing a system’s crystalline symmetries. The Dirac points in Cd₃As₂ and Na₃Bi, as well as the line nodes proposed in Cu₃N and observed in Ca₃P₂^{17,18,33–35}, obey this property, whereas the proposed Dirac points in BiO₂ and the Dirac line nodes in SrIrO₃ do not^{19,37}. We can designate this first category of nodal systems as *band-inversion* semimetals. The nodes in these systems are optional features of the space group; they are certainly locally permitted by crystalline symmetries, or topology in the case of Dirac line nodes under weak spin-orbit interaction, but they are otherwise globally extraneous. Conversely, the nodes in BiO₂ and SrIrO₃ are part of groupings of 4 and 8 bands, respectively. All of the bands in these systems are grouped at a minimum in these numbers, and the existence of nodal features at the Fermi energy appears to be guaranteed by the electron filling. We therefore designate these as *essential* semimetals, or systems with nodes which are pinned into existence by additional space-group-specific symmetries.

This relationship between essential nodal features and filling is, as discussed in this manuscript, the single-particle manifestation of the concept of “minimal insulating filling.” Watanabe, Po, Vishwanath, and Zaletel (WPVZ) realized that for 220 of the 230 space groups, a discussion of related flat compact manifolds allows one to exclude the existence of an insulating state at fillings specific to each space group⁴⁵. In this manuscript, we designate the integer fillings at which WPVZ deduced an allowed insulating state as the “WPVZ bound.” In the limit that interactions are weak and bands are well-defined, we observe that *the same combinations of crystalline symmetries which define the WPVZ bound also*

conspire to guarantee essential groupings of bands. Furthermore, in cases where local topological features might be removed to open a gap, such as the combination of two Weyl points with opposite Chern numbers⁴⁶, this bound provides an obstruction to that process. For example, if two Weyl points are required to exist by minimal insulating filling, they cannot be gapped out while preserving all crystalline symmetries, even if they have opposite Chern numbers, as the bands which comprise them cannot be separated without lowering the system symmetry and changing the space-group-specific filling constraints.

In practice, the determination of this bound, as well as the accompanying analysis of crystalline symmetries in the noninteracting limit, is difficult in three dimensions. Noting that Young and Kane also predicted essential semimetallic features in two-dimensions⁴⁷, we therefore propose a consideration of the WPVZ bound and the allowed nodal features in two dimensions. Furthermore, to restrict our discussion to the role of crystalline symmetries, we require strong spin-orbit interaction, such that locally-protected topological features, such as the Dirac points in graphene, are disallowed. In this paper, we observe that, considering the full set of 80 two-dimensional systems known as the “layer groups”⁴⁸, nontrivial WPVZ bounds can be achieved and rich nodal semimetallic phenomena can be both created in *band-inversion* semimetals and required in *essential* semimetals. Some of these phenomena are protected by the same mechanisms as are their three-dimensional cousins, such as BiO₂ and SrIrO₃. Furthermore, we show how this analysis predicts previously uncharacterized nodal phenomena in two- and three-dimensions, such as band-inversion Dirac points protected by an inversion-center offset and an essential 8-band “cat’s cradle” Weyl fermion feature.

B. Contents of this Manuscript

This paper is structured as follows. First, in II we use a discussion of compact flat manifolds to rederive the WPVZ bound in first purely two-dimensional systems (wallpaper groups) and then in two-dimensional systems embedded in three dimensions (layer groups). Following that, we provide in III a breakdown of the eigenvalue structure of band groupings as it relates to spatial symmetries and inversion centers. Finally, in IV we combine both descriptions to produce criteria for predicting semimetallic features and apply them to a set of related simple models characteristic of both band-inversion and essential nodal semimetallic features in two dimensional crystals with strong spin-orbit interaction.

II. PLATYCOSMS AND MINIMAL INSULATING FILLING

To begin, we relate the idea of minimal insulating filling to the compatibility between a given lattice and a

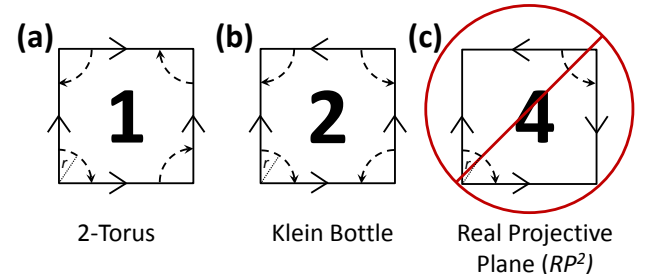


FIG. 1. The 3 compact manifolds which can be achieved by twisting the boundary conditions for a strictly two-dimensional system. The local designations of the perpendicular direction are indicated by the arrows, a notation known as the “fundamental polygon.” Of the possible manifolds, the 2-torus (a) and the Klein bottle (b) are flat, but the real projective plane (RP^2) (c) is not. Flatness can be evaluated by testing for the existence of fixed or special points by drawing a circle centered on the boundary and comparing its circumference to that of a circle drawn on the interior. Starting at the bottom left corner, the dashed line indicates the boundary of a circle of radius r . For the 2-torus and the Klein bottle, this boundary explores all four corners, resulting in a circumference of $2\pi r$, matching the value on the interior. However, for RP^2 , this boundary only additionally explores the top right corner before returning, resulting in a reduced circumference of just πr , and indicating that the two bottom corners are special points, distinct from the interior and from each other, and therefore that RP^2 is not uniform. The bold numbers indicate the number of times that each pattern would have to be repeated to create a supercell with the same boundary conditions as the initial 2-torus. Pictorial guides to forming such supercells can be found in Appendix A.

set of flat compact manifolds. Recent work by Watanabe, Po, Vishwanath, and Zaletel (WPVZ) has revived interest in this relationship between the space groups and three-dimensional manifolds⁴⁵. To introduce this topic, we begin with a review of familiar manifolds in two-dimensions. We then extend this discussion to encompass layered three-dimensional systems. Finally, we conclude this section with a review of the WPVZ arguments for minimal insulating filling and how those arguments relate to the sets of compact flat manifolds in two and three dimensions.

A. Compact Flat Manifolds in Two and Three Dimensions

For a periodic 2D system, say a piece of paper wrapped onto itself, there are two ways to assign boundary conditions for each direction. Linking the two opposite sides without any twists produces a cylinder, and twisting once produces the familiar Möbius strip. Visually, one can assign boundary conditions for such an object by considering the orientation of arrows on the fundamental polygon (Fig. 1). The three distinct combinations of arrow

assignments for a fully-periodic two-dimensional system give a 2-torus, a Klein bottle, and the real projective plane (RP^2). Keeping the arrow assignments consistent relative to the left-hand side of the polygon, one could produce a pattern like the one on a 2-Torus (Fig. 1(a)) by linking together *twice* a Klein bottle (Fig. 1(b)) or *four times* RP^2 (Fig. 1(c)). The creation of such a supercell from the various manifolds is visually depicted in Appendix A.

These manifolds can accommodate the set of truly two-dimensional systems, that is, systems comprised of two-dimensional objects embedded in a two-dimensional space. Some of these manifolds permit the embedding of a subset of lattices known as the *Wallpaper Groups*⁴⁹. When considered in three dimensions, the wallpaper groups consist of the 17 unique lattices that could describe the two-dimensional boundary of a three-dimensional object. They are therefore characterized only by symmetries which preserve the interior and exterior of such a boundary, namely mirror and glide lines in the plane and rotations of the surface about its norm. For this reason, the operation of an arrow flip could also be considered the modding out of a glide mirror, as a site on the left side of a *flipped* boundary is related to a site on the right side by a glide mirror operation.

Modding out a single glide produces the Klein bottle (Fig. 1(b)): a two-dimensional manifold that has just one surface (also sometimes called nonorientable as its surface does not preserve the handedness of a coordinate axis which traverses it)⁵⁰. This object is compact, as it was constructed periodically, and but it is also flat. Modding out an additional glide produces the one-sided real projective plane (RP^2) (Fig. 1(c)), which unlike the 2-torus and Klein bottle has fixed points, and is therefore not flat and uniform.

One can test for these fixed or special points in two dimensions by considering the circumference of a circle of radius r centered throughout the manifold. In the center of all three two-dimensional manifolds, this circle has circumference $2\pi r$. The only possible deviations from this value can occur at the boundaries of the manifolds, as depicted by the dashed lines in Figure 1. For the 2-torus and the Klein bottle, the boundary of a circle of radius r centered at the bottom left corner still explores all three other corners before returning, resulting in a circumference of $2\pi r$, a value that matches circles on the interior. However, for RP^2 , the boundary returns to itself after only reaching the top right corner, giving a circumference of just πr , and indicating that the two bottom corners are special points, different from each other and from the interior.

A key restriction of WPVZ's argument is that any manifold for consideration must allow the uniform embedding of a crystal lattice such that the Bloch wave functions are periodic plane waves⁴⁵. The special corners in RP^2 violate this uniformity, and therefore modding out onto it is disallowed. We therefore conclude that the *wallpaper groups* can only be uniformly embedded on

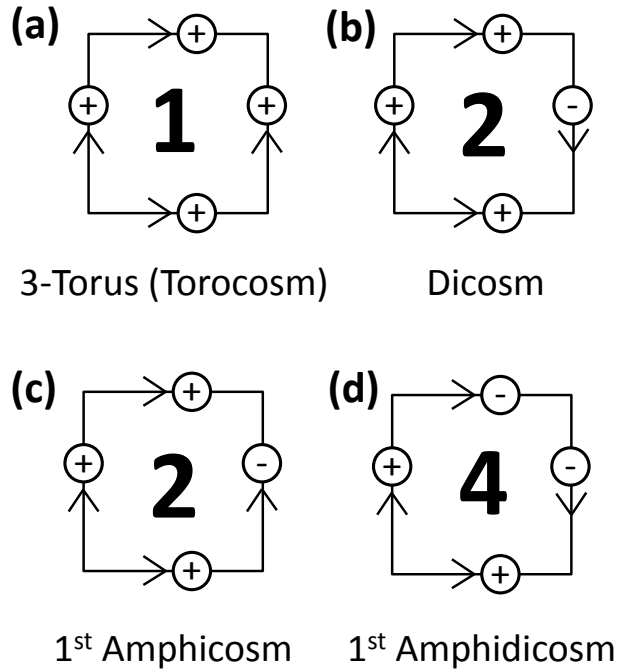


FIG. 2. The compact, flat manifolds which can be achieved in three-dimensional, layered systems. The notation used is a modification of the fundamental polygon from Figure 1 by the additional local assignment of the stacking direction as indicated by the \oplus and \ominus signs. Unlike in the strictly two-dimensional wallpaper systems, the modding out of a two-fold screw is also allowed and leads to a new manifold which doesn't decompose into S^1 multiplied by a wallpaper manifold. Modding a screw preserves the interior and exterior surfaces leading to the dicosm (b). Modding a glide reduces the system to being one-sided and leads to the 1st amphicosm (c). In these layered systems, unlike in the 2D wallpaper cases, a particular combination of two perpendicular nonsymmorphic operations can be modded out without introducing fixed points, leading to a new flat manifold, the 1st amphidicosm (d). The bold numbers indicate the number of times that each pattern would have to be repeated to create a supercell with the same boundary conditions as the initial 3-torus (a). The procedure for forming such supercells is explained with visuals in Appendix A.

the 2-torus and on the Klein bottle.

In three-dimensions, this argument can be extended, though unfortunately in general there is no neat analogue to the fundamental polygon to describe the equivalent operations of modding out glide mirrors or screws. The 10 resultant flat manifolds are known as the platycosms. Descriptions of them, as well as, where possible, connections to more familiar manifolds, are detailed in plain language in Ref. 50.

However, for 80 realizations of the 230 three-dimensional space groups, lattices can be decomposed into two-dimensional sheets, only related to the next layer by crystal periodicity in the stacking direction. For

these layered systems, symmetry-enforced physics is entirely determined by the symmetries of a two-dimensional single layer, and therefore even though they are three-dimensional systems, many of their properties can be determined by confining analysis to the two-dimensional subsystem of a single layer. These single-layer systems, comprised of two-dimensional objects embedded in three dimensions, are a subset of “subperiodic groups” known as the *Layer Groups*⁴⁸.

For these layer group systems, placement onto a platycosm can be visually represented by modifying the fundamental polygon to include a local specification of the \hat{z} direction (stacking direction) (Fig. 2). For these systems the modding out of a two-fold screw is now also permitted in addition to the glide mirror mod, with the screw mod taking one to the two-sided dicosm (Fig. 2(b)) and the glide mod taking one to the one-sided 1st amphicosm (Fig. 2(c)) (which can also be expressed as *klein bottle* $\times S^1$)^{45,50}. Remarkably, the modding out of a glide which flips the \hat{z} direction as well as a perpendicular screw results in a manifold which, unlike RP^2 in the fully-two-dimensional wallpaper systems, is flat. This manifold, the 1st amphidicosm (Fig. 2(d)), actually needs to be placed *four* times to reorient the system boundary to match the torus configuration of the modified fundamental polygon, a property which will have significant band-structure implications. Visual representations of this comparison of the twisted manifolds with the initial torus can be found in Appendix A.

B. Minimal Insulating Filling by Kramer’s Theorem

In Ref. 45, the authors combined an understanding of the platycosms with Kramer’s Theorem to make a strong statement about space-group-symmetry-enforced insulators. In the following text, we reproduce their arguments and then apply them to the restricted set of layer group systems.

For any real system with spinful electrons, there exists a time-reversal operator θ which squares to -1 and mandates, according to Kramer’s theorem, that each state is two-fold degenerate. Under this restriction, a periodic crystal with an odd number of electrons N_e must, independent of how its boundary conditions are applied, have a partially filled state and therefore be a metal or a semimetal⁴⁵. That number of electrons can be expressed as $N_e = N_{cell}\nu$, where N_{cell} is the number of unit cells and ν is the filling per unit cell. Therefore, Kramer’s theorem can be restated as a requirement that $\nu \in 2\mathbb{Z}$ to avoid a metallic state.

Now, when the unit cell is constructed of energetically identical sites related by some spatial operation, one can consider the operation which takes you between sites as a nonsymmorphic symmetry: a combination of a fractional lattice translation and a spatial operation. The quintessential example of a system with such a symme-

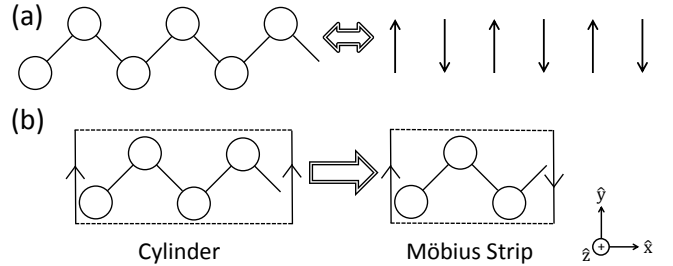


FIG. 3. The nonsymmorphic Su-Schrieffer-Heeger (SSH) Model on a periodic system. All of the information about this system can be encoded by replacing each site with a vector object pointing in the $\pm\hat{y}$ direction (a). When the system has an even number of sites and the boundary condition is not twisted, it lives on a cylinder (b). However, one can produce an electronically equivalent system, if the number of unit cells is large, by removing one site and twisting the boundary condition in the y direction, which places the lattice instead on a Möbius strip.

try is the nonsymmorphic realization of the Su-Schrieffer-Heeger (SSH) model, which is a one-dimensional bipartite chain where the sites can be equivalently represented by a local up or down vector object (Fig. 3(a)). In this SSH model, the nonsymmorphic symmetry which relates the two sites is a mirror of the y direction and a half-lattice translation in the x direction.

On this specific lattice, one could consider taking the final unit cell before the boundary and eliminating one of the sites. This new system with a decimated unit cell, if sufficiently large, will still be equivalent to the original system as long as the boundary condition reproduces the nonsymmorphic symmetry (Fig. 3(b))⁴⁵. However, the resultant crystal now has a fractional N_{cell} (here a half integer), and therefore in this crystal, assembled with this boundary condition, Kramer’s theorem actually requires that $\nu \in 4\mathbb{Z}$ to avoid a metallic state. Stated differently, *four-band models of this system are incapable of being bulk insulators at half filling*.

In systems with more than one periodic direction, there can be multiple nonsymmorphic symmetries to consider. The process of decimating the final unit cell and twisting the boundary condition to reproduce the nonsymmorphic symmetries is in fact just a reproduction of the modding process used to generate the manifolds in Section II A. In 1D (with two-dimensional sites) with this SSH model, the decimation process reduces the underlying manifold from a cylinder to a Möbius strip⁵¹. In two and layered three dimensions, this decimation process exactly corresponds to placing the lattice onto one of the manifolds in Figures 1 and 2 respectively. With multiple nonsymmorphic symmetries, *the condition for flatness is a simple check in these systems whether the product of the two symmetry operations modded out, as defined from a common origin, is itself also an inherently nonsymmorphic operation*. The prefactor on the integer filling to avoid a

metallic state exactly corresponds to the degree of decimation of the final unit cell, expressed as the large bold numbers in Figures 1 and 2. For reference, visual representations of this decimation process for two-dimensional lattices can be found in Appendix A.

In the limit that interactions are weak and bands are well defined, *this minimum filling corresponds to the number of bands which must “stick together,” independent of any band-tuning conditions.* Bands which stick together are bounded by two- and four-fold degeneracies which can only be moved, but not gapped, by tuning space-group-allowed hopping terms. Any band crossings on lines between these degeneracies are therefore also stuck in existence, also only capable of movement but not gapping. Throughout this manuscript, we will relate these groupings of bands to the WPVZ bound for minimal insulating filling established by combining the platycosm modding procedure and Kramer’s theorem.

Finally, WPVZ noted that in three-dimensions, there are a handful of exceptions to the bound established by these arguments, with breakdowns occurring in some cases of multiple nonsymmorphic symmetries or because of unusual, highly degenerate points^{31,32}. However, none of these exceptions occur in the 80 layer groups, and the WPVZ bound therefore in these systems exactly captures the filling restrictions imposed by nonsymmorphic symmetries.

In Appendix C, we list all of the layer groups as well as their corresponding space groups, allowed manifold placements, and insulating filling restrictions.

III. BAND MULTIPLICITY AND EIGENVALUE STRUCTURE

In the band theory limit, the arguments made by WPVZ must still be consistent with any symmetry- or topology-related mechanism for the protection of nodal features. In three-dimensional systems with strong spin-orbit coupling, nodes such as Weyl points can be locally protected by a topological invariant⁴⁶. However, in two dimensions, or in three-dimensional systems with a higher symmetry, the protection of nodal features is frequently determined instead by the local symmetry eigenvalue structure of the bands. In particular, to protect a node, the bands which cross must not share the same symmetry eigenvalues, or in general they will anticross and form a gap.

The set of protected degeneracies in the layer groups with strong spin-orbit interaction, including both essential- and band-inversion-type nodes, is entirely determined by the kinds of allowed band multiplicities and eigenvalue structures. In this section, we review basics regarding the treatment of symmetry operators in k -space, working up to how two-fold symmetries can provide more exotic degeneracies and eigenvalue pairings.

In k -space, we can consider an operation for symmetry evaluation if the rotations, inversions, and time-reverses

in it return k to itself modulo 2π . At a generic, low-symmetry value of k , only the combination of P and θ can be a symmetry. If $\theta^2 = -1$, then $\tilde{\theta}^2 = (P \times \theta)^2 = -1$ enforces Kramer’s theorem for each value of k such that bands everywhere are two-fold degenerate.

Other symmetries are valid along points, lines, and planes and can also lead to two- or even four-fold band multiplets. In this section, we examine the examples of symmetry eigenvalue character which can locally protect a band crossing. We start at the time-reversal-invariant momenta and reduce symmetry from there to planes and lines. We close with a discussion of symmetry eigenvalues, working up from singly-degenerate bands to eigenvalue structures in band multiplets.

A. Time-Reversal-Invariant Momenta

At a Time-Reversal-Invariant crystal Momentum (TRIM), the layer groups will host symmetry-required degeneracies of 2 or 4 bands for systems with time-reversal-symmetry θ . Kramer’s theorem requires that under $\theta^2 = -1$, states at the TRIMs are two-fold degenerate. Additionally, should $\theta|u\rangle \neq \Pi|u\rangle \neq |u\rangle$, where Π is an arbitrary symmetry operation valid at that particular TRIM, the Hamiltonian must have a degeneracy of at least 4. A common example of this relationship between θ and Π occurs with two-fold symmetries, for which *if two spatial operations have representations which commute with time-reversal and anticommute with each other, and at least one of them squares to +1, then states at that TRIM will be 4-fold degenerate*.¹⁹. Four-fold degeneracies can also occur at points owing to the relationship between a spatial symmetry and a rotation of order $n > 2$ ^{17,18}, but in the layer groups, these systems are unable to host many of the *essential nonsymmorphic* nodal features on which this manuscript focuses, and therefore we will restrict ourselves to systems with two-fold rotations.

B. Crystalline Symmetries

Away from the TRIMs, bands along lines and planes can be eigenstates of rotation, mirror, glide mirror, and screw rotation. The eigenvalues of these operations are independent of their position-space origins, though their relative commutation relations, as we will see, are not. Spatial inversion $P(\vec{k} \rightarrow -\vec{k})$, valid only at the TRIMs, does not involve the spin-degree of freedom, and thus independent of the square of time-reversal always has eigenvalues ± 1 . For the remaining operations, we will restrict ourselves to the case where $\theta^2 = -1$. Rotations about an axis ($C_{n\vec{v}}$ where the rotation is through an angle $2\pi/n$ about \vec{v}) have eigenvalues $(-1)^{1/n}$ and are valid along high-symmetry lines in 2D and 3D. Mirror, or an improper rotation, can be considered the product of P and $C_{2\vec{v}}$ and therefore has eigenvalues $\pm i$. Mirrors are

valid along planes in 3D and lines in the layer groups, except for $M_{\vec{z}}$ which is valid for the whole 2D BZ.

A nonsymmorphic operation, a glide or a screw, can be considered as a mirror or a rotation g about some point in space, followed by a fractional lattice translation \vec{t} in a direction such that $g\vec{t} = \vec{t}$. They are valid along the same BZ lines and planes as are their symmorphic counterparts. For a half translation, these operations (rotation or mirror) take on the same eigenvalues as their symmorphic counterparts, $\pm i$, multiplied by $e^{i\vec{k}\cdot\vec{t}}$:

$$\lambda_{2-fold\ NS}^{\pm} = \pm ie^{i\vec{k}\cdot\vec{t}}, \vec{t}\cdot\vec{G} = \pi \quad (1)$$

where \vec{G} is a reciprocal lattice vector such that \vec{t} is a half lattice translation. In the layer groups, the consideration of nonsymmorphic symmetries is greatly simplified as there are *only* two-fold screws and glide mirrors; higher-fold screws or quarter-translation “ d ” glides require some amount of translation or rotation into the stacking or z direction. At the representation level, nonsymmorphic symmetries always have the same square at Γ as their symmorphic counterparts, a value which winds by -1 as one moves along the half-translation direction in the BZ.

As highlighted in Ref. 47, the fractional translation of a nonsymmorphic symmetry gives the nonsymmorphic eigenvalues a k periodicity greater than the 2π of the Brillouin zone. For a half translation, the eigenvalues wind with a 4π periodicity, which dictates that the $+$ and $-$ eigenstates of a glide or a two-fold screw have to connect somewhere along the translation direction and resolve this discrepancy. In fact, this implies that the choice of designating a band as a $+$ or $-$ eigenstate away from Γ is a gauge choice, as the eigenvalues cannot be defined continuously and with period 2π .

This inability to define a 2π -periodic gauge for nonsymmorphic symmetries, and the resolution that bands are required to cross, is in fact the band-theory limit of the WPVZ bound on the minimal insulating filling. For all nonsymmorphic systems, bands can be found in groupings of *no fewer than 4*, and so at fillings other than $4\mathbb{Z}$, these systems are unavoidably metallic. Furthermore, even when nodal features at fillings $\nu \neq 4\mathbb{Z}$ have well-defined topological indexes, such as Chern numbers for Weyl points in three dimensions, this requirement that 4 or more bands must stick together in nonsymmorphic systems obstructs two nodes from combining and gapping out. As we will see in the examples throughout this manuscript, *even if two Weyl points have opposite Chern numbers, they may not be pairwise eliminated if they are part of a nonsymmorphic-symmetry-enforced “band-sticking” feature.*

C. Two- and Four-Fold Band Multiplets

If bands are singly degenerate, then the determination of their symmetry eigenvalues is sufficient in determin-

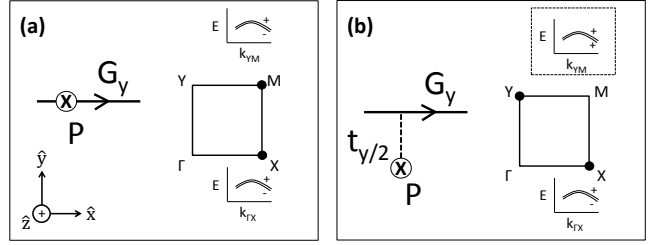


FIG. 4. Possible locations of a glide line G_y relative to an inversion center P in a 2D rectangular system with TRIMs $\Gamma X M Y$. In both cases, for $\theta^2 = -1$ all states are two-fold degenerate because there is a local time-reversal operator $(P\theta)^2 = -1$. If the inversion center is coincident with the glide line (a), there will be four-fold representations at X and M , but all eigenstates of G_y will have eigenvalue pairings $\{+, -\}$ and can never cross. If the inversion center differs from the glide line by a quarter lattice spacing (b), then the operator for G_y will contain an extra $t_{y/2}$ when defined from the common origin of the inversion center, leading to four-fold points instead at X and Y . In this case, then while the states along $\overline{\Gamma X}$ are still paired with G_y eigenvalues $\{+, -\}$, eigenstates along \overline{YM} are paired $\{+, +\}$ or $\{-, -\}$ and are allowed to cross and create four-fold Dirac points with local protection⁵².

ing if they can cross and permit locally-protected nodal features. However, when bands are two- or four-fold degenerate, then one additionally has to determine the symmetry eigenvalue of the local Kramer’s partner. Absent the consideration of rotations of order $n > 2$, a two-fold degenerate state can occur at a point if either the representations of two spatial operations valid at that point anticommute, or if the combination of a spatial operation Π and θ return k to itself at that point *and* $(\Pi \times \theta)^2 = -1$, locally enforcing Kramer’s theorem. Two kinds of spatial operations Π support these conditions: spatial inversion P and two-fold nonsymmorphic symmetries.

When the center of inversion P lies on all mirror and rotation lines, this picture is greatly simplified. Taking $G_y = t_{x/2}M_{\hat{y}}$ on a 2D rectangular lattice as an example, we can first consider the case where the inversion center is coincident with the glide line (Fig. 4(a)). Because both P and θ flip \vec{k} and $P^2 = +1$, all states will be two-fold degenerate for strong spin-orbit systems where $\theta^2 = -1$. However, to evaluate the potential semimetallic properties of this geometry, it is necessary to determine the eigenvalue structure of the G_y eigenstates along $\overline{\Gamma X}$ and \overline{YM} , as well as the locations of any required four-fold Dirac points. We can examine the relationship between P, θ , and G_y as representations on a four-site $\mathcal{H}(\vec{k})$ and use the additional factors of $e^{i\vec{k}\cdot\vec{t}}$ from the full lattice translations \vec{t} to establish commutation relations. Calling the representation of the operator for this case of inversion center location G_y^a , at a TRIM:

$$\begin{aligned}
G_y^a P &= t_{x/2} M_{\hat{y}} P \\
&= P t_{-x/2} M_{\hat{y}} \\
&= t_x P t_{x/2} M_{\hat{y}} \\
G_y^a P &= e^{-ik_x} P G_y^a
\end{aligned} \tag{2}$$

where in the final line we have acted t_{-x} on an eigenstate of G_y . For mathematical consistency, *it was crucial that we have chosen all operations to have the same position-space origin* (here the inversion center). Though this nuance can be overlooked when all mirror planes and lines are coincident with the inversion center, as they are in Ref. 47, *it becomes a central detail when evaluating the eigenvalue character of systems for which one is unable to define a common origin for two spatial symmetries*, as we will see throughout this manuscript. Equation 2 implies that $\{G_y^a, P\} = 0$ at X and M . As $P^2 = +1$ at those points, the emphasized statement in III A implies that representations at those TRIMs must be 4×4 , and thus that all states at X and M are four-fold degenerate (Fig. 4(a)).

Away from the TRIMs, we must additionally determine the eigenvalues of states along G_y glide lines. Considering $|+\rangle$ to be the positive eigenstate of G_y such that:

$$G_y^a |+\rangle = i e^{ik_x/2} |+\rangle \tag{3}$$

whose eigenvalue we compare to the local Kramer's partner $P\theta|+\rangle$:

$$\begin{aligned}
G_y^a (P\theta|+\rangle) &= t_{x/2} M_{\hat{y}} P\theta|+\rangle \\
&= P\theta t_{-x/2} M_{\hat{y}}|+\rangle \\
&= t_x P\theta G_y^a|+\rangle \\
G_y^a (P\theta|+\rangle) &= -i e^{ik_x/2} (P\theta|+\rangle)
\end{aligned} \tag{4}$$

revealing that along both \overline{X} and \overline{Y} all eigenstates of G_y have eigenvalues $\{+, -\}$ and thus can only anticross (Fig. 4(a)).

However, as emphasized in Ref. 52, this picture changes significantly when the inversion center does not lie along a particular mirror or rotation axis. Consider in a 2D rectangular system with a glide line $G_y = t_{x/2} M_{\hat{y}}$ which lies $a_y/4$ above the inversion center (Fig. 4(b)). Therefore, in order to consistently keep the commutation relations of the representations $[P, M_i] = 0$ and $\{C_{2i}, C_{2j}\} = -2\delta_{ij}$ (true for spinful systems where $C_{2i}^2 = -1$), we have to define at the operator level:

$$G_y^b = t_{y/2} t_{x/2} M_{\hat{y}} \tag{5}$$

where G_y^b will here indicate a glide that lies some y -direction displacement from the inversion center. Reevaluating the commutation relations at the TRIMs:

$$\begin{aligned}
G_y^b P &= t_{y/2} t_{x/2} M_{\hat{y}} P \\
&= P t_{-x/2} t_{-y/2} M_{\hat{y}} \\
&= t_x t_y P t_{x/2} t_{y/2} M_{\hat{y}} \\
G_y^b P &= e^{-ik_x} e^{ik_y} P G_y^b
\end{aligned} \tag{6}$$

where the final line is evaluated by acting the translations on an eigenstate of G_y . In this case, $\{G_y^b, P\} = 0$ now at X and Y , which by the arguments in III A requires that all states be four-fold degenerate at those TRIMs (Fig. 4(b)).

Moving off of the TRIMs, we can examine how this inversion center offset affects the eigenvalue character of the local Kramer's partners:

$$\begin{aligned}
G_y^b (P\theta|+\rangle) &= t_{x/2} t_{y/2} M_{\hat{y}} P\theta|+\rangle \\
&= P\theta t_{-x/2} t_{-y/2} M_{\hat{y}}|+\rangle \\
&= t_x t_y P\theta G_y^b|+\rangle \\
G_y^b (P\theta|+\rangle) &= -i e^{ik_x/2} e^{ik_y} (P\theta|+\rangle).
\end{aligned} \tag{7}$$

This implies that along \overline{X} , states still have G_y eigenvalue pairings $\{+, -\}$ and still always anticross. But along \overline{Y} , states are two-fold degenerate with G_y eigenvalues $\{+, +\}$ or $\{-, -\}$, and therefore in that glide line a four-fold crossing can be locally protected (Fig. 4)⁵². However, *we have not specified whether such a crossing must occur*, as is required for example in SrIrO₃ in space group 62³⁷. Such a distinction requires additional information about the nonsymmorphic symmetries present globally across the BZ. In subsequent sections, we will provide both examples of layer group systems where crossings protected by an inversion-center offset are required in *essential* semimetals and optional in *band-inversion* semimetals.

Two-fold degenerate lines and planes can also occur in systems with two-fold nonsymmorphic symmetries^{31,53}. For example, in a rectangular two-dimensional system, the product of $\Pi = t_{x/2} M_{\hat{y}}$ and θ returns \vec{k} to itself along \overline{Y} and \overline{X} . Independent of θ^2 , $(\Pi\theta)^2 = t_x = e^{ik_x}$ when acted on a state, guaranteeing states are at least two-fold degenerate along \overline{X} . In these cases, bands along this line can be two-fold degenerate and have the same or opposite local Kramer's partner eigenvalues, depending on the relative origins of the crystalline symmetries. This can, in at least the case of breaking a double Dirac point in space group 135, lead to an unusual four-fold Dirac semimetal *without* inversion symmetry³¹. In the 2D cases of the layer groups, there may not be enough degrees of freedom to create a system without inversion where this four-fold crossing is the only feature at the Fermi energy.

Four-fold degenerate lines are also occasionally possible in the layer groups. For example, consider a system where along a line two crystalline symmetries Π_1 and Π_2 are valid and states are already required to be two-fold degenerate either by inversion and $\theta^2 = -1$ or by

a two-fold nonsymmorphic symmetry. If $|+\rangle_1$ has the same Π_1 eigenvalue as its local Kramer's partner and if $\{\Pi_1, \Pi_2\} = 0$ along this line, then that guarantees that $\Pi_1|+\rangle_1 \neq \Pi_2|+\rangle_1$. Therefore states along the line are *four-fold* degenerate with Π_1 eigenvalues $\{+, +, -, -\}$.

However, as exhaustively detailed in Ref. 54, a system can only host one four-fold irreducible representation along a line in three dimensions, and therefore also in layer group systems. Two four-fold lines can thus never cross to form a locally-protected eight-fold point along a line in three or fewer dimensions.

IV. SEMIMETALS IN THE LAYER GROUPS

Seeking to examine nodal phenomena from both WPVZ bound and crystalline symmetry perspectives in strong spin-orbit systems in the layer groups, we present a simple model that typifies the layer group systems which contain essential nodal features. In this section, we show how a four-site rectangular lattice can capture a large variety of both essential and band-inversion semimetallic features in two dimensions when its sites are dressed with three-dimensional vector objects, which one can think of as local displacements or dipole moments. After presenting this construction, we sort our models by their WPVZ bound in the platycosm formulation, and show using local eigenvalue character how nodal features are protected. Finally, we show how some of these quasi-two-dimensional systems relate to existing three-dimensional semimetals.

As seen in Figure 5, our model system consists of four sublattices arranged on a rectangular lattice. Describing our sublattice space with Pauli matrices, τ^x describes s-orbital-like hopping between the A and B sites and μ^x describes s-orbital-like hopping between the A and C sites, such that second-neighbor s-like hopping is given by $\tau^x \mu^x$. Each site also has a spin degree of freedom σ which is flipped under $\theta = i\sigma^y K \otimes (\vec{k} \rightarrow -\vec{k})$ for a general $\mathcal{H}(\vec{k})$. This four-site unit cell, like that of any space group with multiple sites per unit cell, can be viewed as originating from a parent high-symmetry Bravais lattice, here a rectangular lattice with spherical sites, followed by the application of a time-reversal-symmetric tensor field (like an electric field) which lowers the periodicity of the system and breaks some subset of point group symmetries at each site⁵⁵. Our model can be realized by choosing just a dipole vector field, such that each site is dressed with a three-dimensional vector object which encodes the underlying crystal symmetries. Physically, this vector can be considered as a local displacement of a single atom or a dipole moment between two atoms.

As one can observe by perusing the table in Appendix C, layer groups with C_{3z} or C_{6z} symmetries can only achieve WPVZ bounds of 2, owing to their inability to host nonsymmorphic symmetries. While these systems can host rotation-protected band-inversion type semimetals, they will not be the focus of this paper. One

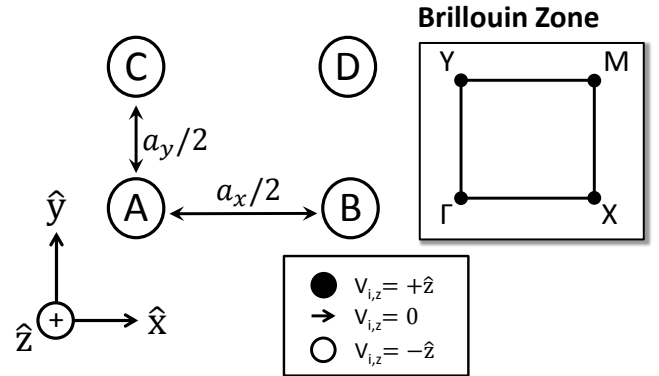


FIG. 5. Four-site model system for semimetals in the layer groups. The four sublattices exist on a 2D rectangular unit cell in the xy plane. Each site has an additional spin degree of freedom. Sites are then dressed with a 3D vector object, visually represented by the symbols in the inset box, which relates them to their neighbors by a symmorphic symmetry operation and a half lattice translation $a_{x/y}/2$. For real systems, this object can represent any time-reversal-symmetric property which transforms as a vector, such as displacement or local dipole moment. By selecting different A-site vectors and lattice generators, a diverse assortment of semimetallic phenomena can be realized. Hamiltonians are generated by considering all first- and second-nearest neighbor hopping terms permitted by the restrictions imposed on $\mathcal{H}(\vec{k})$ by the generators of a particular layer group. The specific terms allowed for each example layer group are detailed in Appendix B.

could consider a system with C_{4z} symmetry as a limiting case of the lattice in Figure 5, in which case our model would collapse onto and recapture the physics in Ref. 47.

Setting first all of the site vectors to $\vec{0}$, we can write down a very high-symmetry Hamiltonian consisting of all possible s-orbital-like hoppings between first- and second nearest neighbors:

$$\begin{aligned} \mathcal{H}_0 = & t_x \cos\left(\frac{k_x}{2}\right) \tau^x + t_y \cos\left(\frac{k_y}{2}\right) \mu^x \\ & + t_2 \cos\left(\frac{k_x}{2}\right) \cos\left(\frac{k_y}{2}\right) \tau^x \mu^x \end{aligned} \quad (8)$$

where we have set the lattice constants $a_x = a_y = 1$ and enforce the inequivalence between x and y by keeping $t_x \neq t_y$. As the on-site vectors are turned on, new hopping terms are allowed, and the symmetry is reduced into a particular layer group. For a given layer group LG , the full second-neighbor Hamiltonian $H_{LG} = H_0 + V_{LG}$ where V_{LG} contains all of the layer-group-specific hopping terms beyond Eq. 8. The details of deriving V_{LG} for each of our examples, as well as layer-group-specific expressions for it, are noted in detail in Appendix B.

As detailed earlier in II A, by allowing placement onto at least one of the four platycosms in Figure 2, layer group systems can achieve a WPVZ bound of 2, 4, or 8 bands sticking together. Within the systems with WPVZ

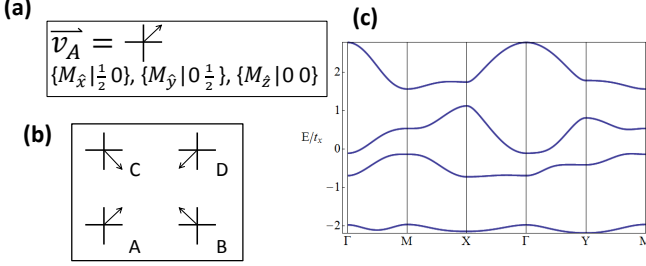
Layer Group 37 (Space Group 47)


FIG. 6. The generators (a), lattice (b), and a typical band structure (c) for *pmmm*, layer group 37, (space group 47). All elements of the layer group are symmorphic, with mirror lines separating the A and B sublattices and A and C sublattices. As the xy plane itself is a mirror, this system is flat and has inversion symmetry, with the inversion center lying at the center of the four sites and at the intersection all 3 mirror lines and planes. Therefore, by the arguments in III C, bands are two-fold degenerate with M_z eigenvalues $\{+, -\}$. Consequently, the bands can only anticross, and at even fillings this system is always an insulator (c).

bounds of 2 and 4, band-inversion metallic and nodal features are also possible for this eight-band model. In the following sections, we present typifying examples for layer group semimetals within each possible WPVZ bound, showing for each example how the WPVZ bound relates to the more familiar crystalline symmetry analysis.

A. WPVZ Bound of 2

Without the presence of a nonsymmorphic symmetry, only time-reversal symmetry can force bands to group together^{19,45,47}. Layer groups with only symmorphic symmetries have band structures with two-fold degeneracies at the time-reversal invariant momenta when $\theta^2 = -1$. Therefore, at half-filling, any system with more than two bands can either be an insulator or a band-inversion semimetal. In the layer groups, there are still myriad ways for a band-inversion crossing to be locally protected by mirror or rotation eigenvalues.

To start, consider the simplest examples, those where the xy -plane itself is a mirror, such that all bands have good M_z quantum numbers. For real materials they correspond to systems which are not buckled or have no additional stacking or external field structure which distinguishes $\pm \hat{z}$, such as graphene without a substrate.

Restricting ourselves to one of these flat layer groups, layer group 37 *pmmm* (which when stacked, is equivalent to space group 47), we first choose an example with only symmorphic symmetries, and therefore a WPVZ bound of 2. The presence of inversion symmetry P, combined with time-reversal makes *all* states two-fold degenerate (Fig. 6). The inversion center lies at the intersection of all three mirror lines and planes (Fig. 6(b)),

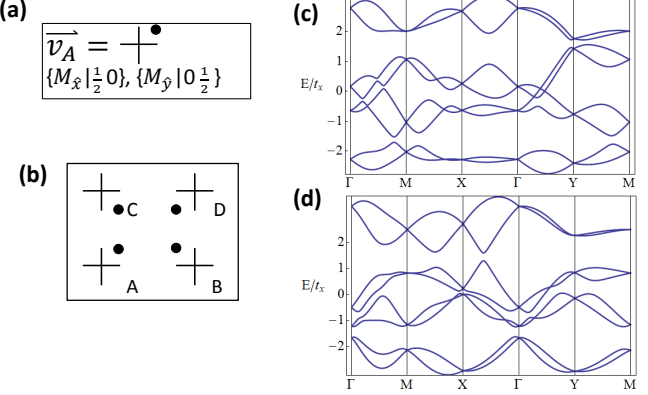
Layer Group 23 (Space Group 25)


FIG. 7. The generators (a), lattice (b), and a typical band structure (c) for *pmm2*, layer group 23, (space group 25). All elements of the layer group are symmorphic, with mirror lines separating the A and B sublattices and A and C sublattices. The vectors have been bent up into the $+\hat{z}$ direction, breaking M_z as one would see if there were a substrate or a perpendicular electric field added to a system in layer group 37 (Fig. 6). Consequently, this system is also a *wallpaper group*, and could describe the surface of a three-dimensional object. Without inversion, nonsymmorphic symmetries, or $n > 2 C_{n\hat{z}}$ rotation points, bands are singly degenerate and can only cross with local protection by mirror eigenvalues on the mirror lines. Typical values of the tight-binding parameters give metallic states at half-filling (c), but values can also be chosen to separate the bands into groups of two and open up gaps at all even fillings (d).

and therefore the local Kramer's partners all of states have opposite mirror eigenvalues, as detailed in III C and Ref. 52. Therefore, regardless of band-tuning conditions, this system will generically be an insulator, because nearby bands can only anticross (Fig. 6(c)).

Conversely, one could imagine putting on an electric field, like that of a substrate, which bends the on-site vectors out of the plane in the $+\hat{z}$ direction. As shown in Figure 7, this reduces the layer group to 23 *pmm2* (space group 25) and breaks M_z and P , allowing for new 1st and 2nd nearest-neighbor hopping terms. As this layer group only consists of in-plane mirrors and rotations about the z axis, it is also one of the *wallpaper* groups described in II A and could be constructed in purely two dimensions, for instance as the surface of a three-dimensional object. States in this layer group are now singly-degenerate, and therefore have the ability to cross with local protection. For typical values of the tight-binding parameters, this system is a band-inversion semimetal (Fig. 7(c)). However, values could also be chosen to open up gaps at all even fillings (Fig. 7(d)), because only sets of two bands are required to stick together by the WPVZ bound.

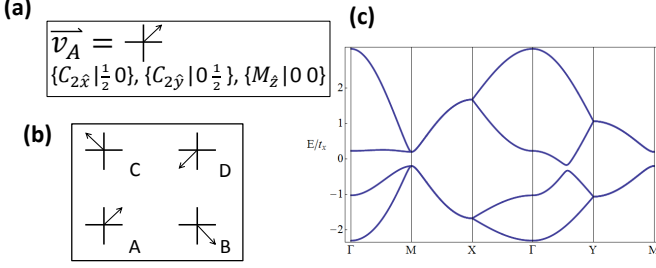
Layer Group 44 (Space Group 55)

FIG. 8. The generators (a), lattice (b), and a typical band structure (c) for *pbam*, layer group 44, (space group 55). This group is a flat layer group generated by constraining into the xy plane a system generated by two perpendicular screws. Consequently, it has inversion symmetry, with the inversion center located in the center of the unit cell, off of the glide lines resulting from the product of P and $S_{2x/y} = t_{x/y/2}C_{2x/y}$. All states are two-fold degenerate by $(P\theta)^2 = -1$ and states along \overline{XM} and \overline{YM} are four-fold degenerate by the combination of glide mirror and M_z , as detailed in III C. States at X , Y , and M are four-fold degenerate due to the relationship between P and $S_{2x/y}$, as detailed in III A and Ref. 47. Therefore, at fillings of $\nu = 2, 6$, this system is an essential Dirac semimetal. States are all paired with symmetry eigenvalues $\{+, -\}$ or in four-fold multiplets, and therefore cannot be tuned to cross by band inversion. Consequently, at half filling ($\nu = 4$), this system is necessarily an insulator.

B. WPVZ Bound of 4

A system with one or more two-fold nonsymmorphic symmetries is allowed placement onto a platycosm other than the 3-torus, and it will therefore host essential groupings of four or eight bands⁴⁵. Within systems with a WPVZ bound of 4, band-inversion semimetals are also possible between groupings of 4 bands, though with additional conditions required for determining if crossings can be locally protected by eigenvalue character. In this section, we first examine two layer groups with a WPVZ bound of 4, which at fillings of $\nu = 2, 6$ are essential Weyl or Dirac semimetals, as explored in Ref. 47. After, we present an example of a band-inversion Dirac semimetal at half filling, protected locally by the inversion center arguments in III C and Ref. 52.

We start with a high-symmetry flat system in layer group 44 *pbam* (space group 55) (Fig. 8). This group is generated by two perpendicular screws protruding from the sites in combination with requiring M_z , which confines the site vectors in the xy plane (Fig. 8(a)). For determining the WPVZ bound, one could either choose the screws and mod out onto the dicosm, or combine a screw with M_z to create a glide line and mod out onto the 1st amphicosm:

$$t_{x/2}C_{2x}M_z = t_{x/2}C_{2x}PC_{2z} = -it_{x/2}PC_{2y} = -i(t_{x/2}M_{\hat{y}}) \quad (9)$$

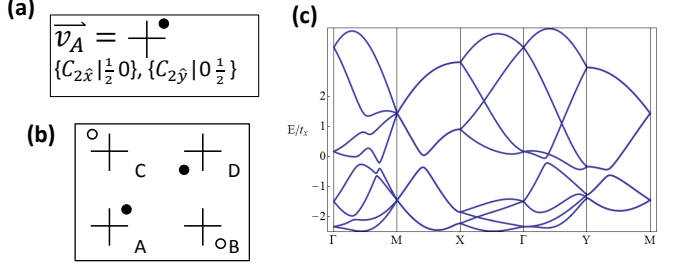
Layer Group 21 (Space Group 18)

FIG. 9. The generators (a), lattice (b), and a typical band structure (c) for $p_21_21_2$, layer group 21, (space group 18). This low-symmetry group is generated just by two perpendicular two-fold screws protruding from the sites. Due to having broken inversion symmetry and a combination of nonsymmorphic symmetries incompatible with placement onto the 1st amphicosm in Fig. 2, this system has 4 bands stick together such that at fillings of $\nu = 2, 6$, it has 2D essential Weyl points along $\overline{\Gamma Y}$ and $\overline{\Gamma Y}^{47}$. Bands along most lines are singly degenerate and therefore capable of crossing with local protection by the same mechanism as in Fig. 6 (though for the choice of parameters in (c) the system is an insulator at half filling; $\overline{\Gamma Y}$ is narrowly gapped). Bands along \overline{XM} and \overline{YM} are two-fold degenerate by the combination of a two-fold nonsymmorphic symmetry and θ , as detailed in III C. M hosts four-fold points despite the absence of inversion, owing to $\{S_{2x}, S_{2y}\} = 0$ and $(S_{2x})^2 = (S_{2y})^2 = +1$ at this point, as detailed in III A.

where we have used the fact that in spinful systems the representations of two-fold rotations obey the same algebra as the Pauli matrices. Either choice of manifold results in a WPVZ bound of 4, a property clearly visible by noting the gap at $\nu = 4$ in the band structure (Fig. 8(c)).

Due to the relationship between two-fold nonsymmorphic symmetries and inversion, highlighted in III A and Ref. 47, the TRIMs at the end of the translation directions (X , Y , and M) all host four-fold degeneracies. Therefore, at fillings of $\nu = 2, 6$, this system is an essential Dirac semimetal. All states are at least two-fold degenerate with symmetry eigenvalues $\{+, -\}$. States along \overline{XM} and \overline{YM} have the requisite offset from the inversion center to have two $+$ eigenvalues, but due to the additionally valid M_z are four-fold degenerate with mirror eigenvalues $\{+, +, -, -\}$, as detailed in III C, and are thus unable to cross. Therefore, at half filling ($\nu = 4$), this system is always an insulator.

We can locally break M_z on the A site and then use the same screws as generators to produce layer group 21 $p_21_21_2$ (space group 18) (Figure 9). In this system, bands are now singly degenerate, except along \overline{XM} and \overline{YM} where they are paired by the combination of θ and a two-fold nonsymmorphic symmetry, as detailed in III C. Bands along $\overline{\Gamma X}$ and $\overline{\Gamma Y}$ feature essential 2D Weyl points⁴⁷, and so consequently, at fillings of $\nu = 2, 6$ this system is a nodal semimetal. As noted in III B, these points cannot be paired at any of the TRIMs and elimi-

nated as long as the two screws are preserved, as the combination of the nonsymmorphic symmetry and $\theta^2 = -1$ provides a topological obstruction to doing so, even when this system is stacked into the third dimension and the Weyl points become 3D with a well-defined Chern number. At M, the two screws anticommute and square to +1, and therefore despite the absence of inversion symmetry, states at M are nevertheless four-fold degenerate. Though we have chosen parameters which gap this system at half filling (Fig. 9(c)), the singly-degenerate bands across many of the high-symmetry lines are capable of inverting with local protection by the same mechanism as the previous WPVZ bound of 2 system, layer group 23 (Fig. 7).

It is worth noting that despite having two perpendicular nonsymmorphic symmetries, layer groups 44 and 21 do not achieve a WPVZ bound of 8. A key requirement of the modding procedure in II A is the choice of manifolds without fixed points. A restatement of this, as noted by Bieberbach, is that *the product of the nonsymmorphic symmetries selected for modding, as defined from a common origin, must itself also be a nonsymmorphic operation*⁵⁰. Examining the two screw generators:

$$t_{x/2}C_{2x}t_{y/2}C_{2y} = it_{x/2}t_{-y/2}(C_{2z}) \quad (10)$$

which is itself just a C_{2z} symmorphic rotation about the center of the unit cell. As we will see in the subsequent section, the only combination of operations which can achieve a WPVZ bound of 8 in layer group systems is $t_{x/2}M_z$ and $t_{y/2}C_{2y}$.

Within the layer groups with a WPVZ bound of 4, one can also achieve a Dirac semimetal at half filling through a band inversion transition. In $p2_1/b11$, layer group 17, (space group 14) (Fig. 10), there exists an offset between horizontal glide lines, which connect adjacent sites A and B, and inversion centers, which lie between sites A and C (Fig. 10(b)). As explained in Ref. 52 and in III C, this causes states along \overline{YM} to be two-fold degenerate with the same glide mirror eigenvalue. A band inversion about a TRIM, here M, leads to the creation of a single Dirac point along \overline{YM} (Fig. 10(d)). In a three-dimensional stack of this system, this feature would instead emerge as a Dirac line node. However, unlike the Dirac line node in SrIrO₃ from Ref. 37, which is also locally protected by an inversion-center offset and a glide mirror, this line node could be removed by a band inversion transition. SrIrO₃ in space group 62 has a WPVZ bound of 8 and is more closely related to a layer group in the following section. Therefore, we find for the protection of essential 8-band Dirac nodal features, the statements from Ref. 52 are necessary for local protection, but insufficient for guaranteeing existence. As we will explore in the following section, an inversion-center offset from a nonsymmorphic symmetry is only one of three conditions required to form an essential Dirac line node. In fact, we will see that 8-band essential semimetallic structures can be formed even in the absence of inversion symmetry.

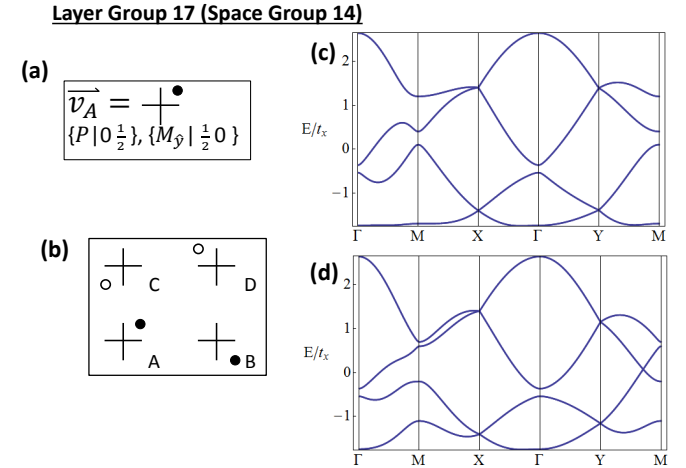


FIG. 10. The generators (a), lattice (b), and two possible band structures (c,d) for $p2_1/b11$, layer group 17, (space group 14). The lattice has horizontal glide lines along the sites and inversion centers between the A and C sites and between the B and D sites. Due to the combination of P and θ , bands everywhere are two-fold degenerate. The offset between the inversion centers and the glide lines leads to four-fold degeneracies at X and Y, as noted in Fig. 4 and in III C. Therefore in accordance with the WPVZ bound, this system is an essential Dirac semimetal at fillings of $\nu = 2, 6$. At half filling, however, it is capable of being both an insulator (c) or a semimetal (d), as bands along \overline{YM} are two-fold degenerate with the same glide mirror eigenvalue. This semimetallic phase is locally protected by the statements in Ref. 52, but can be gapped out by a band inversion transition. Therefore, for guaranteeing the existence of an *essential* 8-band Dirac semimetallic phase, like that in SrIrO₃ in Ref. 37, we find the inversion-center offset highlighted in Ref. 52 to be a necessary, but insufficient condition, and that we must require additional constraints.

C. WPVZ Bound of 8

Though many layer groups exist with multiple perpendicular, two-fold nonsymmorphic symmetries, only 3 such groups exist which satisfy the condition for modding out more than one nonsymmorphic operation, namely that *the product of the two operations, as defined from a common origin, is itself a nonsymmorphic operation*⁵⁰. We find that in the 80 layer groups, only lattices with both $t_{x/2}M_z$ and $t_{y/2}C_{2y}$ (as well as any trivial, in-plane rotations of them) can achieve this condition and therefore allow placement onto the 1st amphidicosm and have a WPVZ bound of 8.

Of these three lattices, two of them, layer groups 43 and 45, have inversion symmetry and are very similar to each other. Choosing to focus on the high-symmetry layer group 45, $pbma$ (Fig. 11), we can see clearly along \overline{XM} a robust 8-band Dirac feature which matches the nodal ring in SrIrO₃³⁷ (Fig. 11(c)). In fact, space group 57, the stacked equivalent of layer group 45, is closely related to the SrIrO₃ $pbnm$ space group 62, with the

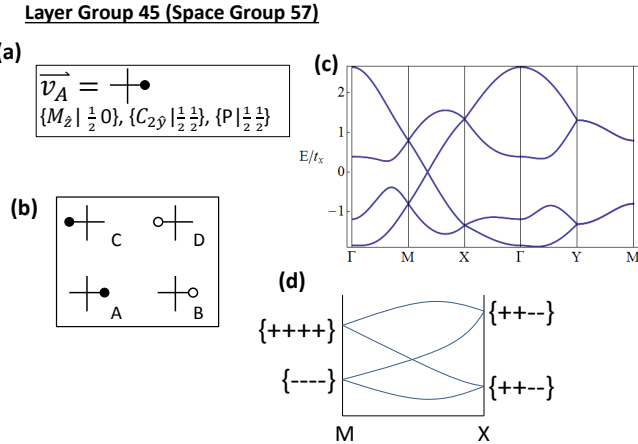


FIG. 11. The generators (a), lattice (b), and a typical band structure (c) for *pbma* layer group 45 (space group 57). This high-symmetry layer group has glide mirrors in the x and z directions and M_y about the sites, such that it has an inversion center in the center of the unit cells, off of glide line $G_x = t_{y/2}M_{\hat{x}}$. This offset allows for bands along \overline{XM} to be two-fold degenerate with the same G_x eigenvalue, which locally protects a Dirac point along that line, much like the local protection of the Dirac point in Fig. 10(d). However, unlike in that semimetal, which is optionally created by tuning through a band inversion transition, the Dirac point in layer group 45 is *essential*, making it more like the essential Dirac line node in SrIrO_3 in space group 62³⁷. Because four-fold points are required at X and M by the relationship between G_x , $S_y = t_{x/2}t_{y/2}C_{2y}$, and P , and because G_x commutes with all other elements of the space group at M , four-fold points at X and M have differing G_x eigenvalue pairings (d), leading to the required crossing along \overline{XM} .

chief difference coming from the substitution of a three-dimensional “n-glide” with an in-plane “b-glide”.

The relationship between layer group 45 and space group 62 can be examined both from a consideration of allowed flat manifold placements and from an evaluation of band multiplicity and symmetry eigenvalue structure. In the language of WPVZ, layer group 45 (space group 57) has a four-site unit cell with nonsymmorphic symmetries $t_{x/2}M_z$ and $t_{y/2}C_{2y}$ as defined from the common origin of the midpoint between the A and B sites, leading as explained in II A an allowed placement onto the 1st amphidicosm and the requirement that 8 bands stick together. Space group 62 has a four-site unit cell with its S_y above the glide plane, so using the same axes one can mod out the nonsymmorphic operations $t_{x/2}M_z$ and $t_{z/2}t_{y/2}C_{2y}$, allowing placement onto the 2nd amphidicosm and requiring that eight bands stick together (the 2nd amphidicosm is a fundamentally three-dimensional manifold and does not neatly decompose into the modified fundamental polygons from Fig. 2.) Neither space group 57 nor space group 62 are among the 10 known examples where the WPVZ bound is insufficient⁴⁵.

From a symmetry perspective, the story regarding this

band structure is a bit more involved. First, for consideration of whether the Dirac point is allowed by local protection, one must check whether there exist any nonsymmorphic operations off of an inversion center, as detailed in III C and Ref. 52. This allows for each band multiplet to have the same nonsymmorphic eigenvalue so that they can possibly cross without gapping out. Next, one needs to check whether states at the ends of the plane or line defined by this inversion center offset, here X and M are four-fold degenerate, either by considering the relationship with inversion and nonsymmorphic symmetries for *all* of the independent combinations of space group elements, as detailed in III A, or by consulting a crystalline symmetry textbook such as Bradley and Cracknell⁵⁴. Finally, if these two conditions are met, one needs to evaluate the eigenvalue structure of the TRIM at which the nonsymmorphic operation in question squares to +1. *If at that TRIM that nonsymmorphic operation commutes with all other operations which complete the space group, then it must have at that point a 4×4 representation proportional to the identity and therefore eigenvalues $\{+, +, +, +\}$ or $\{-, -, -, -\}$.* Matching the bands between the two TRIMs, two sets of two-fold bands must cross creating an *essential* Dirac point. In three dimensions, if this occurs in a glide plane, then any path between the two TRIMs must contain a Dirac crossing and a Dirac line node forms, as is the case in SrIrO_3 . Elements of these criteria for this particular iridate system were recently noted in Ref. 38.

Returning to layer group 45, we can examine how evaluating these criteria works in practice. Only the product of two generators, $G_x = t_{y/2}M_{\hat{x}}$, satisfies the inversion-center-offset criterion and is therefore suitable for consideration. States at X must therefore be four-fold degenerate, as $\{G_x, P\} = 0$ here and $P^2 = +1$, as noted in III A. At M , another two-fold operation, such as $t_{y/2}C_{2y}$, as defined from an inversion center, leads to the requirement that states there also be four-fold degenerate. Finally, we can note that as defined from a common origin along the G_x lines, $[G_x, \Pi] = 0$ at M , where Π stands for any remaining independent element of the layer group other than G_x . Matching bands with the same G_x eigenvalues, Fig. 11(d) shows that these criteria require the existence of a Dirac point along \overline{XM} .

While more involved than the WPVZ method for determining if eight bands have to stick together in a system with inversion symmetry, this consideration of symmetry eigenvalues and commutation relations is beneficial when dealing with three-dimensional space groups for which the WPVZ bound breaks down. For example, in systems where high-fold rotation leads to an eight-fold double Dirac point, the WPVZ bound only seems to capture the particular 8-band Dirac feature from layer group 45. While the WPVZ bound states that space group 130 has a minimal insulating filling of $8\mathbb{Z}$ and space group 135 a minimal insulating filling of $4\mathbb{Z}$, both crystal systems are very similar in practice and both in practice host essential double Dirac points³¹. The only distinguishing

feature between them is that additional Dirac points are present at the Fermi energy in space group 130, owing to the offset of a screw rotation from the inversion centers. The same set of two-fold nonsymmorphic symmetries lies along the inversion centers in space group 135, and therefore the first part of the criteria for local protection of such a Dirac point is not met.

This consideration of two-fold nonsymmorphic symmetries predicts 8-band Dirac features even when the WPVZ bound fails. Space group 73, due to the limitations of the modding procedure as it relates to inversion symmetry, combined with the body-centered shape of its unit cell, is incorrectly predicted to have a minimal insulating filling of $4\mathbb{Z}$ by the platycosm formulation of the WPVZ bound⁴⁵. In a paper released during the final stages of preparing this manuscript, WPVZ noted using a similar eigenvalue and commutation algebra procedure that this system, generated only by two-fold nonsymmorphic symmetries, hosts essential eight-band features in the noninteracting limit⁵⁷.

The WPVZ bound proves most significant when considering systems without inversion. In layer group 33 pb_21a (space group 29) (Fig. 12(a)), there is no inversion symmetry, and so bands can only become two-fold degenerate by the combination of θ and a two-fold nonsymmorphic symmetry (here $G_x = t_{x/2}t_{y/2}M_{\hat{x}}$ for \overline{YM}) or by the anticommutativity of two spatial symmetries along a common line (here $S_y = t_{y/2}C_{2y}$ and G_x along $\overline{Y\Gamma}$) (Fig. 12(c)). However, neither set of two-fold-degenerate bands contributes to obvious eight-band essential Dirac features, and one might be tempted when just considering symmetry eigenvalues to guess that this layer group is an insulator at $\nu = 4$. However, because this four-site system has S_y and $G_z = t_{x/2}M_{\hat{z}}$, placement is still allowed onto the 1st amphidicosm and WPVZ predicts that eight bands stick together. Observing the band structure (Fig. 12(c)), there is in fact an *essential eight-band, “cat’s cradle-like” Weyl feature* present along the path $\overline{\Gamma X} \cup \overline{XM}$.

These essential Weyl points can be explained by examining the evolution of nonsymmorphic symmetry eigenvalues (Fig. 12(d)). Along $\overline{\Gamma X}$, a band with G_z eigenvalue $+i$ at Γ has to have eigenvalue -1 at X by the choice of nonsymmorphic eigenvalue gauge $\lambda_{\pm} = \pm ie^{ik_x/2}$. This leads to characteristic four-band Weyl features along $\overline{\Gamma X}$ ⁴⁷. Along \overline{XM} , however, $[G_z, S_y] = 0$. Therefore, even though the eigenstates of S_y will form the same characteristic four-band Weyl features as they evolve from X to M , they will exchange partners which keep the same G_z eigenvalue (Fig. 12(d)). As bands with differing eigenvalues of G_z (labeled in (Fig. 12(d)) with dashed or solid lines) can cross with local protection, this guarantees that the bands along $\overline{\Gamma X}$ and \overline{XM} are stuck together in sets of eight. Should one choose to tune parameters such that the bands along \overline{XM} are separated at half filling, then the bands will instead cross along $\overline{\Gamma X}$.

Layer Group 33 (Space Group 29)

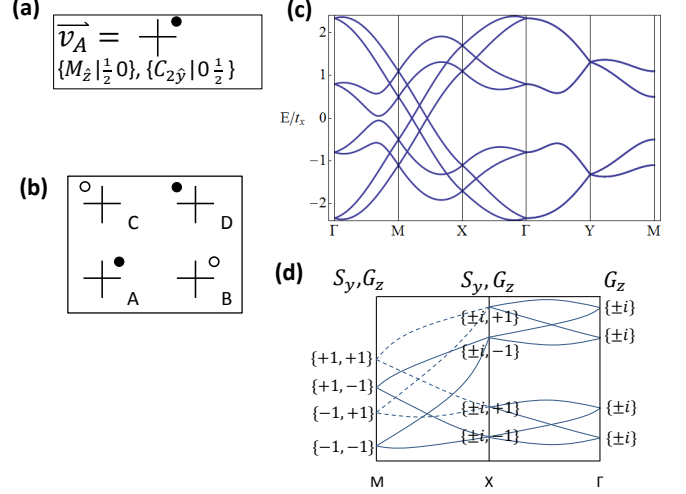


FIG. 12. The generators (a), lattice (b), and a typical band structure (c) for layer group 33 pb_21a (space group 29). This is the only layer group which can achieve a WPVZ bound of 8 without inversion symmetry. States along $\overline{Y\Gamma}$ are two-fold degenerate by the anticommutativity of $S_y = t_{y/2}C_{2y}$ and $G_x = t_{x/2}t_{y/2}M_{\hat{x}}$. States along \overline{YM} are two-fold degenerate by the combination of G_x and θ . Even though the layer group only consists of two-fold nonsymmorphic symmetries without inversion, the combination of symmetries is such that eight bands have to stick together along $\overline{\Gamma X}$ and \overline{XM} . Listing the eigenvalues of S_y and $G_z = t_{x/2}M_{\hat{z}}$ (d), the evolution of the two-fold nonsymmorphic eigenvalues for each symmetry $\lambda_{\pm} = \pm ie^{ik_x/y/2}$ causes bands to form characteristic four-band structures as explained in Ref. 47. Starting at Γ , one can choose parameters such that along $\overline{\Gamma X}$ there is a gap at half filling with these four-band structures above and below the gap. However, because $[S_y, G_z] = 0$ along \overline{XM} , the four-band structures which form along \overline{XM} preserve the eigenvalue of G_z ($\pm i$ indicated as a dashed or solid line respectively) and exchange new partners with local protection, forming a sort of 8-band “cat’s cradle” structure and filling in the gap at $\nu = 4$ with essential Weyl points. Should one tune parameters as to open up a gap along \overline{XM} , the resultant Weyl points at half filling will instead form along $\overline{\Gamma X}$.

V. DISCUSSION

In this paper, we have fully characterized the essential nodal semimetallic band features allowed in the layer groups. By using a bound on the minimal insulating filling, which derives from the ability to place the underlying lattice onto a flat compact manifold, we found that there can be layer group semimetals with 2, 4, or 8 bands required to “stick together,” band groupings which cannot be removed without lowering the spatial symmetry of the system. This bound was achieved following a procedure by Watanabe, Po, Vishwanath, and Zaletel (WPVZ) in Ref. 45 valid for both interacting and noninteracting systems which, though failing in select cases in

three dimensions^{31,32,57}, is complete for all of the space groups which derive from trivial stackings of the wallpaper and layer groups. Within those layer groups with a minimal insulating filling of $4\mathbb{Z}$, the results of Ref. 47 can be recovered, but one can also find new features, such as a band-inversion-type Dirac semimetal protected by an inversion-center offset. Three layer group systems, specifically layer groups 33, 43, and 45 (space groups 29, 54, and 57, respectively, when stacked) can achieve a minimal insulating filling of $8\mathbb{Z}$. Layer groups 54 and 57 have inversion symmetry, and are therefore Dirac semimetals at half filling, with their 8-band essential Dirac features owing to the same mechanism of symmetry protection as the line node in SrIrO_3 ³⁷. Layer group 33, however, does not have inversion, and instead has a previously uncharacterized essential eight-band “cat’s cradle” Weyl fermion feature with two essential Weyl points present along a high-symmetry line at half filling.

In addition to the constraints imposed on the band features of quasi-two-dimensional mono- or few-layer systems, this consideration of compact flat manifold placements, specifically for the strictly two-dimensional wallpaper systems in II A, also provides restrictions on the allowed band features on the surfaces of three-dimensional systems. Specifically, for groupings of bands which don’t require a bulk to exist, namely the trivially-connected states of topological crystalline insulators, such as the “hourglass fermions” in Ref. 58, this bound indicates that *at most, four bands can be forced by symmetry to stick together on the surface of a three-dimensional system*. As there are only four wallpaper groups with glide lines, this further constrains the possible topological surface band flows as well. Considering the allowed band features in the wallpaper groups, a combination of symmetry analysis and minimal insulating filling restrictions should allow one to exhaustively deduce all possible “hourglass”-like surface flows permitted in bulk-insulating systems.

Finally, the two-dimensional and quasi-two-dimensional systems characterized in this paper can provide significant benefits over their three-dimensional counterparts. They are considerably easier to visualize and analyze by crystalline symmetry. They are also easier to simulate in tight-binding and density functional theory calculations, allowing for a relatively fast route towards predicting and engineering two-dimensional nodal semimetals, including eight-band structures analogous to those in three dimensions. These systems can also allow experimental access to two-dimensional topological physics. As characterized in Ref. 47, nonsymmorphic two-dimensional materials can be pinned by an additional symmetry to the quantum critical point between a trivial and a topological insulator, and therefore one could consider them as parent materials for examining strain-engineered topological phase transitions.

We thank Toen Castle, Randall Kamien, Youngkuk Kim, and Andrew M. Rappe for helpful discussions. This work was supported by NSF grant DMR 1120901 and a Simons Investigator grant to CLK from the Simons

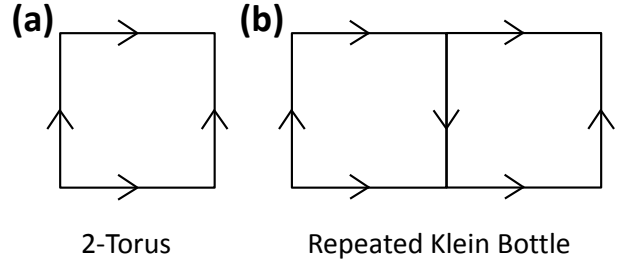


FIG. 13. A 2-torus (a) and two Klein bottles with a common boundary (b). In order to create a shape with the same external arrows as the 2-torus, two Klein bottles have to be placed together, sharing the common twisted boundary. This procedure is the origin of the bold numbers in Figures 1 and 2. For a four-site unit cell, this decimation factor, $n_{dec} = A_{unit}/A_{dec}$ where A is the area of the original and decimated unit cells respectively, gives the minimal insulating filling constraint $\nu \in 2n_{dec}\mathbb{Z}$.

Foundation.

Appendix A: Further Notes on and Examples of Decimations and Flat-Manifold Placement

In this appendix, we visually detail the decimation procedure from Figure 3 in layered two-dimensional systems.

For layered two-dimensional systems, the consideration of minimal insulating filling is, for most systems, captured by the number of fixed-point-free decimations of a four-site unit cell. One can consider this unit cell as being the final one before the boundary in both the x and y (in plane) directions. As one row of atoms is chopped off and the boundary condition twisted, this unit cell is decimated by modding out the nonsymmorphic symmetry which related the atoms remaining to those removed by decimation. We can consider for any manifold a decimation factor:

$$n_{dec} = \frac{A_{unit}}{A_{dec}} \quad (\text{A1})$$

which measures the ratio of the areas of the original to the decimated unit cell. This factor is precisely the bold numbers indicated in Figures 1 and 2, which could also be expressed as the number of times a manifold would have to be repeated with a common boundary in order to create a supercell with the same external boundary as the 2-torus in wallpaper systems, or the 3-torus in general layer group systems (Figure 13). For a four-site unit cell in two-dimensions, the insulating fillings, absent any additional band inversions, are therefore:

$$\nu \in 2n_{dec}\mathbb{Z}. \quad (\text{A2})$$

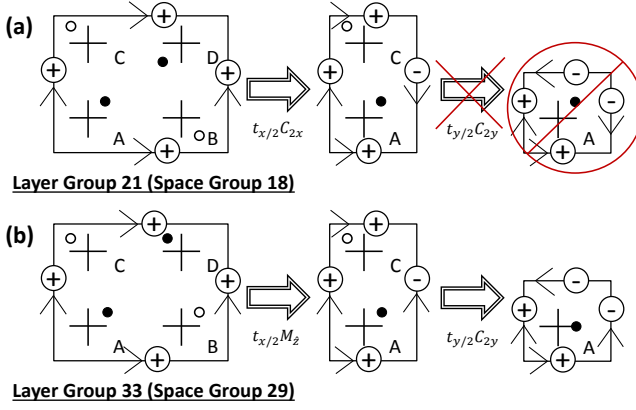


FIG. 14. A demonstration of the decimation procedure for two layer groups with multiple nonsymmorphic symmetries. The minimal insulating filling is proportional to the ratio of the sizes of the maximally decimated unit cell to that of the original, with special consideration given to avoid decimations which introduce fixed points. Layer group 21 (space group 18) (a) is generated by two perpendicular screws: $S_{x/y} = t_{x/y/2}C_{2x/y}$. One could choose to mod out S_x first, reducing the area of the unit cell by half and placing the system onto the dicosm. However, further decimation by S_y would then be disallowed, because $S_xS_y \sim t_{x/2}t_{y/2}(C_{2z})$, which is an inherently *symmetric* operation (C_{2z} about the center of the unit cell). Therefore, choosing either screw, the maximal decimation of layer group 21 gives $n_{dec} = 2$ and placement onto the dicosm, with a minimal insulating filling of $\nu \in 4\mathbb{Z}$. Conversely, layer group 33 (space group 29) (b) is generated by S_y and $G_z = t_{x/2}M_z$. Modding out G_z first removes the right half of the unit cell and places the system onto the 1st amphidicosm. However, this is not the maximal decimation, as the product $S_yG_z \sim t_{x/2}(t_{y/2}M_z)$, which is an inherently *nonsymmorphic* operation. Therefore, layer group 33 admits an additional decimation by S_y onto the 1st amphidicosm, resulting in $n_{dec} = 4$ and a minimal insulating filling of $\nu \in 8\mathbb{Z}$.

The key part of this procedure is the restriction that we only utilized fixed-point-free decimations. As emphasized in the main text, *multiple decimations by two-fold operations are only allowed if the product of those operations is itself also an inherently nonsymmorphic operation*^{45,50}.

Figure 14 illustrates two examples of layer groups with multiple nonsymmorphic group elements. Layer group 21 (space group 18) (Fig. 14(a)) is generated by two perpendicular screws: $S_{x/y} = t_{x/y/2}C_{2x/y}$. One could choose to mod out S_x first, reducing the area of the unit cell by half and placing the system onto the dicosm. However, further decimation by S_y would then be disallowed, because $S_xS_y \sim t_{x/2}t_{y/2}(C_{2z})$, which is an inherently *symmetric* operation (C_{2z} about the center of the unit cell). Therefore, choosing either screw, the maximal decimation of layer group 21 gives $n_{dec} = 2$ and placement onto the dicosm, with a minimal insulating filling of $\nu \in 4\mathbb{Z}$. Conversely, layer group 33 (space group 29) (Fig. 14(b)) is generated by S_y and $G_z = t_{x/2}M_z$. Modding out G_z first removes the right half of the unit

cell and places the system onto the 1st amphidicosm. However, this is not the maximal decimation, as the product $S_yG_z \sim t_{x/2}(t_{y/2}M_z)$, which is an inherently *nonsymmorphic* operation. Therefore, layer group 33 admits an additional decimation by S_y onto the 1st amphidicosm, resulting in $n_{dec} = 4$ and a minimal insulating filling of $\nu \in 8\mathbb{Z}$.

Appendix B: Tight Binding Models

In this appendix, we list the tight-binding Hamiltonians for the example layer groups selected for this manuscript (Figs. 6-12).

We begin by considering a four-site rectangular unit cell in two-dimensions (Fig. 5). Initially, each site has spherical symmetry such that this high-symmetry system can be considered a relabeling of a rectangular one-site unit cell with all of the symmetries of the underlying Bravais lattice. Repeating the procedure from IV, we designate Pauli matrices to for the sublattice degrees of freedom, with τ^x indicating s-orbital-like hopping between the A and B (and C and D) sites and μ^x indicating s-orbital-like hopping between the A and C sites (and B and D) such that $\tau^x\mu^x$ indicates s-like-hopping between A and D sites (and B and C). Each site is given an additional spin degree of freedom σ such that our overall model has eight bands.

We can, in this high-symmetry limit, first write down all of the first- and second-nearest-neighbor s-orbital-like hopping terms:

$$\begin{aligned} \mathcal{H}_0 = & t_x \cos\left(\frac{k_x}{2}\right) \tau^x + t_y \cos\left(\frac{k_y}{2}\right) \mu^x \\ & + t_2 \cos\left(\frac{k_x}{2}\right) \cos\left(\frac{k_y}{2}\right) \tau^x \mu^x \end{aligned} \quad (\text{B1})$$

where the lattice spacing $a_{x/y}$ has been set to 1. From there, terms can be added to reduce the symmetry of the system into a particular layer group and lift many of the degeneracies. For a particular layer group LG , we consider the set of all symmetry-allowed first- and second-nearest-neighbor hoppings (other than the existing s-like ones) to be a potential V_{LG} such that overall $\mathcal{H}_{LG} = \mathcal{H}_0 + V_{LG}$. We find that using all of the terms up to second-nearest-neighbor interactions produces layer-group-specific band structures (though occasionally allows for an artificial chiral symmetry, which could be broken by introducing symmetry-allowed third-nearest-neighbor terms.)

For each layer group, the allowed terms V_{LG} can be determined by considering how the group generators transform a generic Hamiltonian $\mathcal{H}(k_x, k_y)$ and finding all physical hopping terms invariant under that transformation. In practice, the form of the representation of each group generator in the sublattice and Bloch space is that of the representation at Γ multiplied by an operation on

\vec{k} . Additionally, all systems are considered to be time-reversal symmetric with $\theta = i\sigma^y K \otimes (\vec{k} \rightarrow -\vec{k})$ such that $\theta^2 = -1$.

In the following subsections, we detail the group generators and V_{LG} for each of the example systems in the text. All generators are defined from the common origin of site A. In order, the generators are described by the name of the generator, the generator as operations defined from site A, and the form of the representation of the operator for our eight-band $\mathcal{H}(\vec{k})$. Similar terms are grouped under the same constants for simplicity, though this is not explicitly required by symmetry. Values of the constants used for band plots have been noted after each V_{LG} .

1. Layer Group 37

Layer group 37, *pmmm* (space group 47) has a WPVZ bound of 2 and the following generators:

$$\begin{aligned} M_{\hat{x}} &= t_{x/2}M_{\hat{x}} = \tau^x\sigma^x \otimes (k_x \rightarrow -k_x) \\ M_{\hat{y}} &= t_{y/2}M_{\hat{y}} = \mu^x\sigma^y \otimes (k_y \rightarrow -k_y) \\ M_{\hat{z}} &= M_{\hat{z}} = \sigma^z. \end{aligned} \quad (B2)$$

This results in the following allowed first- and second-nearest-neighbor hopping terms:

$$\begin{aligned} V_{37} = \cos\left(\frac{k_x}{2}\right) &[v_{r1x}\tau^y\mu^z\sigma^z] \\ + \sin\left(\frac{k_x}{2}\right) &[v_{p1x}\tau^y + v_{s1x}\tau^x\mu^z\sigma^z] \\ + \cos\left(\frac{k_y}{2}\right) &[v_{r1y}\tau^z\mu^y\sigma^z] \\ + \sin\left(\frac{k_y}{2}\right) &[v_{p1y}\mu^y + v_{s1y}\tau^z\mu^x\sigma^z] \\ + \sin\left(\frac{k_x}{2}\right)\cos\left(\frac{k_y}{2}\right) &[v_{p2}\tau^y\mu^x] \\ + \cos\left(\frac{k_x}{2}\right)\sin\left(\frac{k_y}{2}\right) &[v_{p2}\tau^x\mu^y] \\ + \sin\left(\frac{k_x}{2}\right)\sin\left(\frac{k_y}{2}\right) &[v_{p2}\tau^y\mu^y]. \end{aligned} \quad (B3)$$

For the bands in Fig. 6(c),

$$\begin{aligned} t_x &= 1.0, \quad t_y = 1.25, \quad t_2 = 0.4, \quad v_{r1x} = 0.3, \\ v_{p1x} &= 0.35, \quad v_{s1x} = -0.65, \quad v_{r1y} = 0.45, \quad v_{p1y} = 0.65 \\ v_{vs1y} &= -0.8, \quad v_{p2} = -0.2. \end{aligned} \quad (B4)$$

2. Layer Group 23

Layer group 23, *pmm2* (space group 25), has a WPVZ bound of 2. It is the result of breaking $M_{\hat{z}}$ in layer group 37, leading to the following generators:

$$\begin{aligned} M_{\hat{x}} &= t_{x/2}M_{\hat{x}} = \tau^x\sigma^x \otimes (k_x \rightarrow -k_x) \\ M_{\hat{y}} &= t_{y/2}M_{\hat{y}} = \mu^x\sigma^y \otimes (k_y \rightarrow -k_y). \end{aligned} \quad (B5)$$

The allowed terms in layer group 23 can be therefore considered as those allowed for layer group 37, plus new terms which don't commute with σ^z :

$$\begin{aligned} V_{23} = V_{37} &+ \cos\left(\frac{k_x}{2}\right)[v_{r1x}\tau^y\sigma^y] + \sin\left(\frac{k_x}{2}\right)[v_{s1x}\tau^x\sigma^y] \\ &+ \cos\left(\frac{k_y}{2}\right)[v_{r1y}\mu^y\sigma^x] + \sin\left(\frac{k_y}{2}\right)[v_{s1y}\mu^x\sigma^x] \\ &+ \cos\left(\frac{k_x}{2}\right)\cos\left(\frac{k_y}{2}\right)[v_{r2}(\tau^x\mu^y\sigma^x + \tau^y\mu^x\sigma^y)] \\ &+ \sin\left(\frac{k_x}{2}\right)\cos\left(\frac{k_y}{2}\right)[v_{s2}(\tau^x\mu^x\sigma^y + \tau^y\mu^y\sigma^x)] \\ &+ \cos\left(\frac{k_x}{2}\right)\sin\left(\frac{k_y}{2}\right)[v_{s2}(\tau^x\mu^x\sigma^x + \tau^y\mu^y\sigma^y)] \\ &+ \sin\left(\frac{k_x}{2}\right)\sin\left(\frac{k_y}{2}\right)[v_{r2}(\tau^x\mu^y\sigma^y + \tau^y\mu^x\sigma^x)]. \end{aligned} \quad (B6)$$

For the bands in Fig. 7(c),

$$\begin{aligned} t_x &= 1.0, \quad t_y = 1.25, \quad t_2 = 0.1, \quad v_{r1x} = 0.3, \\ v_{p1x} &= 0.35, \quad v_{s1x} = -0.65, \quad v_{r1y} = 0.45, \quad v_{p1y} = 0.65 \\ v_{vs1y} &= 0.7, \quad v_{p2} = -0.2, \quad v_{s2} = -0.35, \quad v_{r2} = 0.3. \end{aligned} \quad (B7)$$

For the bands in Fig. 7(d),

$$\begin{aligned} t_x &= 1.0, \quad t_y = 1.25, \quad t_2 = 0.9, \quad v_{r1x} = 0.3, \\ v_{p1x} &= 0.35, \quad v_{s1x} = -0.65, \quad v_{r1y} = 0.45, \quad v_{p1y} = 0.65 \\ v_{vs1y} &= 0.7, \quad v_{p2} = -0.9, \quad v_{s2} = -0.35, \quad v_{r2} = 0.1. \end{aligned} \quad (B8)$$

3. Layer Group 44

Layer group 44, *pbam* (space group 55) has a WPVZ bound of 4 and the following generators:

$$\begin{aligned} S_x &= t_{x/2}C_{2x} = \tau^x\sigma^x \otimes (k_y \rightarrow -k_y) \\ S_y &= t_{y/2}C_{2y} = \mu^x\sigma^y \otimes (k_x \rightarrow -k_x) \\ M_{\hat{z}} &= M_{\hat{z}} = \sigma^z. \end{aligned} \quad (B9)$$

This results in the following allowed first- and second-nearest-neighbor hopping terms:

$$\begin{aligned} V_{44} = & \cos\left(\frac{k_x}{2}\right) [v_{r1x}\tau^y\mu^z\sigma^z] + \cos\left(\frac{k_y}{2}\right) [v_{r1y}\tau^z\mu^y\sigma^z] \\ & + \sin\left(\frac{k_x}{2}\right) \cos\left(\frac{k_y}{2}\right) [v_{p2}\tau^x\mu^y] \\ & + \cos\left(\frac{k_x}{2}\right) \sin\left(\frac{k_y}{2}\right) [v_{p2}\tau^y\mu^x] \\ & + \sin\left(\frac{k_x}{2}\right) \sin\left(\frac{k_y}{2}\right) [v_{p2}\tau^y\mu^y]. \end{aligned} \quad (\text{B10})$$

For the bands in Fig. 8(c),

$$\begin{aligned} t_x = 1.0, \quad t_y = 1.55, \quad t_2 = 0.4, \quad v_{r1x} = 0.3, \\ v_{vr1y} = 0.6, \quad v_{p2} = 0.2. \end{aligned} \quad (\text{B11})$$

4. Layer Group 21

Layer group 21, $p\bar{2}_1\bar{2}_12$ (space group 18), has a WPVZ bound of 4. It is the result of breaking M_z in layer group 44, leading to the following generators:

$$\begin{aligned} S_x = t_{x/2}C_{2x} &= \tau^x\sigma^x \otimes (k_y \rightarrow -k_y) \\ S_y = t_{y/2}C_{2y} &= \mu^x\sigma^y \otimes (k_x \rightarrow -k_x). \end{aligned} \quad (\text{B12})$$

The allowed terms in layer group 21 can be therefore considered as those allowed for layer group 44, plus new terms which don't commute with σ^z :

$$\begin{aligned} V_{21} = V_{44} &+ \cos\left(\frac{k_x}{2}\right) [v_{r1x}(\tau^y\sigma^y + \tau^y\mu^z\sigma^z)] \\ &+ \sin\left(\frac{k_x}{2}\right) [v_{s1x}\tau^x\sigma^x] \\ &+ \cos\left(\frac{k_y}{2}\right) [v_{r1y}(\mu^y\sigma^x + \tau^z\mu^y\sigma^z)] \\ &+ \sin\left(\frac{k_y}{2}\right) [v_{s1y}\mu^x\sigma^y] \\ &+ \cos\left(\frac{k_x}{2}\right) \cos\left(\frac{k_y}{2}\right) [v_{r2}(\tau^x\mu^y\sigma^x + \tau^y\mu^x\sigma^y)] \\ &+ \sin\left(\frac{k_x}{2}\right) \cos\left(\frac{k_y}{2}\right) [v_{s2}(\tau^x\mu^x\sigma^x + \tau^y\mu^y\sigma^y)] \\ &+ \cos\left(\frac{k_x}{2}\right) \sin\left(\frac{k_y}{2}\right) [v_{s2}(\tau^x\mu^x\sigma^y + \tau^y\mu^y\sigma^x)] \\ &+ \sin\left(\frac{k_x}{2}\right) \sin\left(\frac{k_y}{2}\right) [v_{r2}(\tau^x\mu^y\sigma^y + \tau^y\mu^x\sigma^x)]. \end{aligned} \quad (\text{B13})$$

For the bands in Fig. 9(c),

$$\begin{aligned} t_x = 1.0, \quad t_y = 1.55, \quad t_2 = 0.4, \quad v_{r1x} = 0.3, \\ v_{s1x} = 0.65, \quad v_{vr1y} = 0.6, \quad v_{s1y} = 0.85, \\ v_{r2} = 0.6, \quad v_{s2} = 0.7. \end{aligned} \quad (\text{B14})$$

5. Layer Group 17

Layer group 17, $p\bar{2}_1/b11$ (space group 14) has a WPVZ bound of 4 and the following generators:

$$\begin{aligned} P = t_{y/2}P &= \mu^x \otimes (\vec{k} \rightarrow -\vec{k}) \\ G_y = t_{x/2}M_{\hat{y}} &= \tau^x\sigma^y \otimes (k_y \rightarrow -k_y). \end{aligned} \quad (\text{B15})$$

This results in the following allowed first- and second-nearest-neighbor hopping terms:

$$\begin{aligned} V_{17} = & \cos\left(\frac{k_x}{2}\right) [v_{r1x}\tau^y\sigma^x] + \sin\left(\frac{k_x}{2}\right) [v_{s1x}\tau^x\mu^z\sigma^y] \\ & + \sin\left(\frac{k_y}{2}\right) [v_{p1y}\tau^z\mu^y] \\ & + \cos\left(\frac{k_x}{2}\right) \cos\left(\frac{k_y}{2}\right) [v_{r2}\tau^y\mu^x\sigma^x] \\ & + \sin\left(\frac{k_x}{2}\right) \cos\left(\frac{k_y}{2}\right) [v_{p2}\tau^x\mu^y + v_{s2}\tau^y\mu^y\sigma^x] \\ & + \cos\left(\frac{k_x}{2}\right) \sin\left(\frac{k_y}{2}\right) [v_{s2}\tau^y\mu^y\sigma^y] \\ & + \sin\left(\frac{k_x}{2}\right) \sin\left(\frac{k_y}{2}\right) [v_{r2}\tau^y\mu^x\sigma^y] \end{aligned} \quad (\text{B16})$$

noting that additional terms are also allowed due to this system's invariance under $\sigma^x \leftrightarrow \sigma^z$.

For the bands in Fig. 10(c),

$$\begin{aligned} t_x = 1.0, \quad t_y = 1.14, \quad t_2 = 0.4, \quad v_{r1x} = 0.3, \\ v_{s1x} = 0.65, \quad v_{vp1y} = 0.8, \quad v_{r2} = 0.25, \\ v_{p2} = 0.2, \quad v_{s2} = 0.45. \end{aligned} \quad (\text{B17})$$

For the bands in Fig. 10(d),

$$\begin{aligned} t_x = 1.0, \quad t_y = 1.14, \quad t_2 = 0.4, \quad v_{r1x} = 0.3, \\ v_{s1x} = 0.65, \quad v_{vp1y} = 0.2, \quad v_{r2} = 0.25, \\ v_{p2} = 0.2, \quad v_{s2} = 0.45. \end{aligned} \quad (\text{B18})$$

6. Layer Group 45

Layer group 45, $pbma$ (space group 57) has a WPVZ bound of 8 and the following generators:

$$\begin{aligned}
G_z &= t_{x/2} M_{\hat{z}} = \tau^x \sigma^z \\
S_y &= t_{x/2} t_{y/2} C_{2y} = \tau^x \mu^x \sigma^y \otimes (k_x \rightarrow -k_x) \\
P &= t_{x/2} t_{y/2} P = \tau^x \mu^x \otimes (\vec{k} \rightarrow -\vec{k}). \quad (B19)
\end{aligned}$$

This results in the following allowed first- and second-nearest-neighbor hopping terms:

$$\begin{aligned}
V_{45} &= \cos\left(\frac{k_x}{2}\right) [v_{r1x} \tau^y \mu^z \sigma^y] + \cos\left(\frac{k_y}{2}\right) [v_{r1y} \tau^z \mu^y \sigma^y] \\
&+ \sin\left(\frac{k_y}{2}\right) [v_{s1y} \tau^z \mu^x \sigma^x] \\
&+ \sin\left(\frac{k_x}{2}\right) \cos\left(\frac{k_y}{2}\right) [v_{p2} \tau^x \mu^y]. \quad (B20)
\end{aligned}$$

For the bands in Fig. 11(c),

$$\begin{aligned}
t_x &= 1.0, \quad t_y = 1.25, \quad t_2 = 0.4, \quad v_{r1x} = -0.3, \\
v_{r1y} &= 0.45, \quad v_{s1y} = 0.8, \quad v_{p2} = -0.2. \quad (B21)
\end{aligned}$$

7. Layer Group 33

Layer group 33, $pb\bar{2}_1a$ (space group 29) has a WPVZ bound of 8 and the following generators:

$$\begin{aligned}
G_z &= t_{x/2} M_{\hat{z}} = \tau^x \sigma^z \\
S_y &= t_{y/2} C_{2y} = \mu^x \sigma^y \otimes (k_x \rightarrow -k_x). \quad (B22)
\end{aligned}$$

$$\begin{aligned}
V_{33} &= \cos\left(\frac{k_x}{2}\right) [v_{r1x} \tau^y \mu^z \sigma^x] + \sin\left(\frac{k_x}{2}\right) [v_{s1x} \tau^x \sigma^z] \\
&+ \cos\left(\frac{k_y}{2}\right) [v_{r1y} (\tau^z \mu^y \sigma^x + \mu^y \sigma^z)] \\
&+ \sin\left(\frac{k_y}{2}\right) [v_{s1y} \tau^z \mu^x \sigma^y] \\
&+ \cos\left(\frac{k_x}{2}\right) \cos\left(\frac{k_y}{2}\right) [v_{r2} (\tau^y \mu^x \sigma^y + \tau^x \mu^y \sigma^z)] \\
&+ \sin\left(\frac{k_x}{2}\right) \cos\left(\frac{k_y}{2}\right) \times \\
&\quad [v_{p2} \tau^x \mu^y + v_{s2} (\tau^y \mu^y \sigma^y + \tau^x \mu^x \sigma^z)] \\
&+ \cos\left(\frac{k_x}{2}\right) \sin\left(\frac{k_y}{2}\right) [v_{s2} \tau^y \mu^y \sigma^x] \\
&+ \sin\left(\frac{k_x}{2}\right) \sin\left(\frac{k_y}{2}\right) [v_{r2} \tau^y \mu^x \sigma^x]. \quad (B23)
\end{aligned}$$

For the bands in Fig. 12(c),

$$\begin{aligned}
t_x &= 1.0, \quad t_y = 1.25, \quad t_2 = 0.4, \quad v_{r1x} = -0.3, \\
v_{s1x} &= 0.3, \quad v_{r1y} = 0.45, \quad v_{s1y} = 0.8, \\
v_{r2} &= 0.25, \quad v_{p2} = -0.2, \quad v_{s2} = 0.45. \quad (B24)
\end{aligned}$$

Appendix C: List of Filling Conditions for the 80 Layer Groups

In this appendix, we list the 80 layer groups as sorted by their allowed platycosm placements. For each layer group, we cite the equivalent space group for a three-dimensional stack of that system⁴⁸.

The 17 layer groups which could additionally describe the boundary of a three-dimensional object also comprise the *wallpaper groups* and are denoted with (w). These groups contain no operations which would exchange the interior and exterior of such a three-dimensional object, and therefore (if \hat{z} is the layer stacking direction or surface normal) are disallowed from having P , $M_{\hat{z}}$, or $C_{2x/y}$, as well as any of those operations plus a translation.

Layer groups without nonsymmorphic symmetries are only allowed placement onto the torocosm, or 3-torus, and have no insulating filling constraints besides $\nu \in 2\mathbb{Z}$ by Kramer's theorem.

3-Torus (43 Layer Groups)			
$\nu \in 2\mathbb{Z}$			
Layer Group	Space Group	Layer Group	Space Group
1 (w)	1	53	89
2	2	55 (w)	99
3 (w)	3	57	111
4	6	59	115
6	10	61	123
8	3	65 (w)	143
10	5	66	147
11 (w)	6	67	149
13 (w)	8	68	150
14	10	69 (w)	156
18	12	70 (w)	157
19	16	71	162
22	21	72	164
23 (w)	25	73 (w)	168
26 (w)	35	74	174
27	25	75	175
35	35	76	177
37	47	77 (w)	183
47	65	78	187
49 (w)	75	79	189
50	81	80	191
51	83		

Layer groups with two-fold screws and no glide mirrors can be decimated and placed onto the two-sided dicosm, which results insulating fillings of $\nu \in 4\mathbb{Z}$ absent any additional band inversions with locally-protected crossings (otherwise stated as the “minimal-insulating filling”).

Only Dicosm (6 Layer Groups) $\nu \in 4\mathbb{Z}$				
Layer Group	Space Group	Layer Group	Space Group	
9	4		21	18
15	11		54	90
20	17		58	113

Layer groups with glide mirrors and no two-fold screws can be decimated and placed onto the one-sided 1st amphicosm, which results in a minimal insulating filling of $\nu \in 4\mathbb{Z}$.

Only 1st Amphicosm (17 Layer Groups) $\nu \in 4\mathbb{Z}$				
Layer Group	Space Group	Layer Group	Space Group	
5	7		36	39
7	13		38	49
12 (w)	7		39	50
16	13		48	67
24 (w)	28		52	85
25 (w)	32		56 (w)	100
30	27		60	117
31	28		62	125
34	30			

Layer groups with both glide mirrors and two-fold screws require more careful examination. As part of the procedure for decimation from II and Appendix A, all combinations of perpendicular nonsymmorphic symmetries must be examined to determine if further decimation is allowed from the dicosm or 1st amphicosm into the 1st amphidicosm. *For the layer groups, that decimation is in practice only allowed for systems with four or more*

sites per unit cell and any z-axis rotation of $S_y = t_{y/2}C_{2y}$ and $G_z = t_{x/2}M_z$.

Absent these conditions, for layer groups with both glide mirrors and screws, frequently the case in those with inversion symmetry, one could choose to mod out using either the glide or the two-fold screw, allowing placement onto either the dicosm or the 1st amphidicosm. For both cases, the filling restrictions are the same: an insulator can only occur at fillings of $\nu \in 4\mathbb{Z}$.

Dicosm or 1st Amphicosm (11 Layer Groups) $\nu \in 4\mathbb{Z}$				
Layer Group	Space Group	Layer Group	Space Group	
17	14		42	53
28	26		44	55
29	26		46	59
32	31		63	127
40	51		64	129
41	51			

Finally, these conditions for further decimation onto to the one-sided 1st amphidicosm are, in fact, only satisfied by 3 layer groups. For these groups, eight bands have to stick together, and therefore they have a minimal insulating filling of $\nu \in 8\mathbb{Z}$.

1st Amphidicosm (3 Layer Groups) $\nu \in 8\mathbb{Z}$				
Layer Group	Space Group	Layer Group	Space Group	
33	29		45	57
43	54			

- ¹ S. Adler, Phys. Rev. **177**, 2426 (1969)
- ² H. B. Nielsen and M. Ninomiya, Phys. Rev. B **130**, 389 (1983).
- ³ D. T. Son and B. Z. Spivak, Phys. Rev. B **88**, 104412 (2013).
- ⁴ M. Fujita, K. Wakabayashi, and K. Nakada, J. Phys. Soc. Jpn. **65**, 1920 (1996).
- ⁵ K. Nakada, M. Fujita, G. Dresselhaus, and M. S. Dresselhaus, Phys. Rev. B **54**, 17954 (1996).
- ⁶ C. L. Kane and E. J. Mele, Phys. Rev. Lett. **95**, 226801 (2005).
- ⁷ L. Fu, C. L. Kane, and E. J. Mele, Phys. Rev. Lett. **98**, 106803 (2007).
- ⁸ P. R. Wallace, Phys. Rev. **71**, 622 (1947).
- ⁹ A. H. Castro Neto, F. Guinea, N. M. R. Peres, K. S. Novoselov, and A. K. Geim, Rev. Mod. Phys. **81**, 109 (2009).
- ¹⁰ A. H. Castro Neto, F. Guinea, N. M. R. Peres, K. S. Novoselov, and A. K. Geim, Rev. Mod. Phys. **81**, 109 (2009).
- ¹¹ E. McCann and V. I. Fal'ko, Phys. Rev. Lett. **96**, 086805

- (2006).
- ¹² F. Zhang, J. Jung, G. A. Fiete, Q. Niu, and A. H. MacDonald, Phys. Rev. Lett. **106**, 156801 (2011).
- ¹³ T. Ohta, A. Bostwick, T. Seyller, K. Horn, and E. Rotenberg, Science **313**, 951 (2006).
- ¹⁴ J. B. Oostinga, H. B. Heersche, X. Liu, A. F. Morpurgo, and L. M. K. Vandersypen, Nature Materials **7**, 151 (2007).
- ¹⁵ H. Min, B. Sahu, S. K. Banerjee, and A. H. MacDonald, Phys. Rev. B **75**, 155115 (2007).
- ¹⁶ B. J. Wieder, F. Zhang, and C. L. Kane, Phys. Rev. B **92**, 085425 (2015).
- ¹⁷ S. Borisenko, Q. Gibson, D. Evtushinsky, V. Zabolotnyy, B. Büchner, and R. J. Cava, Phys. Rev. Lett. **113**, 027603 (2014).
- ¹⁸ Z. K. Liu, B. Zhou, Y. Zhang, Z. J. Wang, H. M. Weng, D. Prabhakaran, S. Mo, Z. X. Shen, Z. Fang, X. Dai, Z. Hussain, and Y. L. Chen, Science **343**, 864 (2014).
- ¹⁹ S. M. Young, S. Zaheer, J. C. Y. Teo, C. L. Kane, E. J. Mele, and A. M. Rappe, Phys. Rev. Lett. **108**, 140405 (2012).
- ²⁰ J. A. Steinberg, S. M. Young, S. Zaheer, C. L. Kane, E.

- J. Mele, and A. M. Rappe, Phys. Rev. Lett. **112**, 036403 (2014).
- ²¹ Y. Chen and H. Kee, Phys. Rev. B **90**, 195145 (2014).
- ²² T. c. v. Bzdušek, A. Rüegg, and M. Sigrist, Phys. Rev. B **91**, 165105 (2015).
- ²³ C. Fang, M. J. Gilbert, X. Dai, and B. A. Bernevig, Phys. Rev. Lett. **108**, 266802 (2012).
- ²⁴ X. Wan, A. M. Turner, A. Vishwanath, and S. Y. Savrasov, Phys. Rev. B **83**, 205101 (2011).
- ²⁵ L. Yang, Z. Liu, Y. Sun, H. Peng, H. Yang, T. Zhang, B. Zhou, Y. Zhang, Y. Guo, M. Rahn, *et al.*, Nature Physics **11**, 728 (2015).
- ²⁶ C. Lee, S. Xu, S. Huang, D. S. Sanchez, I. Belopolski, G. Chang, G. Bian, N. Alidoust, H. Zheng, M. Neupane, B. Wang, A. Bansil, M. Z. Hasan, and H. Lin, Phys. Rev. B **92**, 235104 (2015).
- ²⁷ M. Hirayama, R. Okugawa, S. Ishibashi, S. Murakami, and T. Miyake, Phys. Rev. Lett. **114**, 206401 (2015).
- ²⁸ S. Huang, S. Xu, I. Belopolski, C. Lee, G. Chang, B. Wang, N. Alidoust, G. Bian, M. Neupane, C. Zhang, S. Jia, A. Bansil, H. Lin, and M. Z. Hasan, Nature Communications **6**, 7373 (2015).
- ²⁹ S. Xu, I. Belopolski, N. Alidoust, M. Neupane, G. Bian, C. Zhang, R. Sankar, G. Chang, Z. Yuan, C. Lee, S. Huang, H. Zheng, J. Ma, D. S. Sanchez, B. Wang, A. Bansil, F. Chou, P. P. Shibayev, H. Lin, S. Jia, and M. Z. Hasan, Science **349**, 613 (2015).
- ³⁰ S. Xu, N. Alidoust, I. Belopolski, Z. Yuan, G. Bian, T. Chang, H. Zheng, V. N. Strocov, D. S. Sanchez, G. Chang, C. Zhang, D. Mou, Y. Wu, L. Huang, C. Lee, S. Huang, B. Wang, A. Bansil, H. Jeng, T. Neupert, A. Kaminski, H. Lin, S. Jia, and M. Z. Hasan, Nature Physics **11**, 748 (2015).
- ³¹ B. J. Wieder, Y. Kim, A. M. Rappe, and C. L. Kane, Phys. Rev. Lett. **116**, 186402 (2016).
- ³² B. Bradlyn, J. Cano, Z. Wang, M. G. Vergniory, C. Felser, R. J. Cava, B. A. Bernevig, Science (2016).
- ³³ Y. Kim, B. J. Wieder, C. L. Kane, and A. M. Rappe, Phys. Rev. Lett. **115**, 036806 (2015).
- ³⁴ R. Yu, H. Weng, Z. Fang, X. Dai, and X. Hu, Phys. Rev. Lett. **115**, 036807 (2015).
- ³⁵ L. S. Xie, L. M. Schoop, E. M. Seibel, Q. D. Gibson, W. Xie, and R. J. Cava, APL Mater. **3**, 083602 (2015).
- ³⁶ G. Bian, T. Chang, R. Sankar, S. Xu, H. Zheng, T. Neupert, C. Chiu, S. Huang, G. Chang, I. Belopolski, D. S. Sanchez, M. Neupane, N. Alidoust, C. Liu, B. Wang, C. Lee, H. Jeng, A. Bansil, F. Chou, H. Lin, and M. Z. Hasan, arXiv:1505.03069 (2015).
- ³⁷ J. Carter, V. V. Shankar, M. A. Zeb, H. Kee, Phys. Rev. B **85**, 115105 (2012).
- ³⁸ Y. Chen, H. Kim, and H. Kee, Phys. Rev. B **93**, 155140 (2016).
- ³⁹ G. E. Volovik, arXiv:1110.4469 (2011).
- ⁴⁰ H. Weng, Y. Liang, Q. Xu, R. Yu, Z. Fang, X. Dai, and Y. Kawazoe, Phys. Rev. B **92**, 045108 (2015).
- ⁴¹ Y. Chen, Y. Xie, S. A. Yang, H. Pan, F. Zhang, M. L. Cohen, and S. Zhang, Nano Lett. **15**, 6974 (2015).
- ⁴² M. Zeng, C. Fang, G. Chang, Y.-A. Chen, T. Hsieh, A. Bansil, H. Lin, and L. Fu, arXiv:1504.03492 (2015).
- ⁴³ D. Gosálbez-Martínez, I. Souza, and D. Vanderbilt, Phys. Rev. B **92**, 085138 (2015).
- ⁴⁴ H. Weng, C. Fang, Z. Fang, B. A. Bernevig, and X. Dai, Phys. Rev. X **5**, 011029 (2015).
- ⁴⁵ H. Watanabe, H. C. Po, A. Vishwanath, and M. Zaletel, PNAS **112**, 47 (2015).
- ⁴⁶ X. Wan, A. M. Turner, A. Vishwanath, and S. Y. Savrasov, Phys. Rev. B **83**, 205101 (2011).
- ⁴⁷ S. M. Young and C. L. Kane, Phys. Rev. Lett. **115**, 126803 (2015).
- ⁴⁸ E. Hitzer and D. Ichikawa, Electronic Proc. of AGACSE 3, Leipzig, Germany (2008).
- ⁴⁹ J. H. Conway, H. Burgiel, and C. Goodman-Strauss, “The Symmetries of Things” (Worcester MA, 2008).
- ⁵⁰ J. H. Conway and J. P. Rossetti, arXiv:math/0311476 (2003).
- ⁵¹ This SSH model uses 2D sites with one periodic dimension, making it a member of the *Frieze Groups*⁴⁸. Like with the layer groups, Frieze group systems are allowed embedding onto manifolds with the dimensionality of their sites. If the sites were one-dimensional, everything would be trivially embedded on a circle (S^1).
- ⁵² C. Fang, Y. Chen, H. Kee, and L. Fu, Phys. Rev. B **92**, 081201 (2015).
- ⁵³ C. Fang, L. Lu, J. Liu, L. Fu, arXiv:1512.01552 (2015).
- ⁵⁴ C. J. Bradley and A. P. Cracknell, “The Mathematical Theory of Symmetry in Solids” (Clarendon Press Oxford, 1972).
- ⁵⁵ Choosing a time-reversal-breaking field, such as a pseudovector magnetic field, is also allowed. Instead of generating the 230 space groups, this leads rather to the 1651 magnetic space groups⁵⁶.
- ⁵⁶ D. B. Litvin, “Magnetic Group Tables” (International Union of Crystallography, 2013).
- ⁵⁷ H. Watanabe, H. C. Po, A. Vishwanath, and M. Zaletel, arXiv:1603.05646 (2016).
- ⁵⁸ Z. Wang, A. Alexandradinata, R. J. Cava, B. A. Bernevig, Nature **532**, 189 (2016).